Veena et al., 2009). Furthermore, chronic stress accelerates cognitive impairments and increases amyloid deposition in APPV717I-CT100 mice overexpressing the familial AD (FAD) V717I "London" mutation within the carboxyl terminus of human amyloid precursor protein (Jeong et al., 2006). However, the combinatorial effect of chronic stress and mutated genes on the hippocampal neurogenesis is not fully understood. Here we hypothesize that, in individuals predisposed to genetic mutations for AD, a mutated gene–environmental stress interaction might synergistically deteriorate the level of hippocampal neurogenesis, leading to precocious cognitive impairment. To test this hypothesis, we selected a transgenic mouse model of AD with overexpression of an FAD-type PS1 (L286V) (L/V-Tg); these mice accumulate abnormal amyloid β in the cytoplasm to bring about massive cell degeneration without formation of amyloid plaques after 6 months of age (Chui et al., 1999). We exposed this genetically predisposed mouse to stressful environments and found that the number of degenerating neurons was increased in the brain regions involved in cognitive function (i.e., the hippocampus) earlier in stressed mice than in non-stressed mice, and neurogenesis was affected differently by stress in the Tg and non-Tg mice. These data suggest that diverse responses to stressful experiences among genetically predisposed individuals might affect neurogenesis and neurodegeneration. We propose that mice that display hallmarks of AD late in life with conditioned environmental factors could be used as an animal model for the analysis of the onset and progression of AD.

Materials and methods

Animals

A transgenic mouse line overexpressing human PS1 with an FAD-related mutation of leucine 286 to valine (L286V) under the control of the human PDGF-β promoter (Chui et al., 1999) had been originally produced by Dr. Chui et al. at the National Institute of Neuroscience (NCNP, Tokyo, Japan). The mouse line was maintained in the FVB/N background and was back-crossed to obtain male hemizygous mice (L/V-Tg) at the NCNP. In the brains of transgenic mice older than 13 months (aged mice), neurodegeneration was significantly accelerated without amyloid plaque formation, whereas most populations of neurons deposit amyloid β42 intracellularly. Mice were housed under controlled conditions (21 °C room temperature, 60% humidity, lights on from 8:00 am to 8:00 pm) with food and water available *ad libitum*. Sixty-two young adult (7-week-old) male mice were used in the whole study. All studies were performed by comparing the L/V-Tg mice with the age-matched, transgenic-negative littermates (non-Tg). The Non-Tg and L/V-Tg mice were randomly assigned to the control (NS) or stressed (ST) group [for short-term experiments, non-Tg(NS) ($n=12$), non-Tg(ST) ($n=12$), L/V-Tg(NS) ($n=13$), L/V-Tg (ST) ($n=13$); for long-term experiments, non-Tg(NS) ($n=3$), non-Tg(ST) ($n=3$), L/V-Tg(NS) ($n=3$), L/V-Tg(ST) ($n=3$)]. Animal care and handling were in accordance with institutional regulations and were approved by the Animal Investigation Committee of the National Institute of Neuroscience, Japan, which in turn conforms to the National Institutes of Health guidelines for the care and use of laboratory animals. The number of animals in this study was the minimum required to obtain statistically significant results. The animals were appropriately treated and anesthetized with Nembutal (Dainippon Sumitomo Pharma Co., Osaka, Japan, 0.25 mg/g of pentobarbitone) to minimize their suffering.

Chronic intermittent restraint stress (CIRS)

Young adult (7-week-old) male mice weighing 25.4±0.5 g for L/V-Tg mice and 24.4±0.5 g for non-Tg mice at the beginning of the stress procedure were used. Mice were housed two to three per cage and were habituated to the experimental room for 10 days without handling. The stressed animals were exposed to restraint stress from 9:30 am to 3:30 pm in their home cage using a well-ventilated restraint tube that fit closely to the mice (Supplementary Fig. 1). For chronic intermittent restraint stress (CIRS), the experimental mice were put into restraint tubes for 6 h every day for 3 weeks (short-term experiments) or 15 weeks (long-term experiments), excluding the weekends (restrained Monday through Friday, rest from 3:30 pm on Friday to 9:30 am on the next Monday). The animals at 11-week-old (short-term) or 23-week-old (long-term) were sacrificed 1 day after the last session (Saturday; Fig. 1). The control mice (NS) were left in their home cage except for handling during weighing and were sacrificed at the same time as the experimental mice (we considered the NS a handled control). Body weight gain was monitored throughout the experiment (three times a week) and, upon termination, the adrenal glands were removed and weighed.

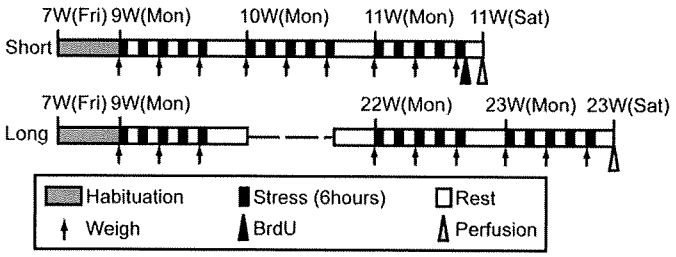

Fig. 1. Protocol summary for short-term (upper) and long-term (lower) chronic intermittent restraint stress (CIRS). For CIRS, each mouse was put into a restraint tube for 6 h every day for 3 weeks (short-term) or 15 weeks (for long-term), excluding weekends, and sacrificed 1 day after the last session (Saturday). For 5-bromo-2′-deoxyuridine (BrdU) labeling, the mice were injected intraperitoneally with BrdU 20 h (for short-term) before perfusion. Fri, Friday; Mon, Monday; Sat, Saturday; W, week-old.

Fixation and histological processing

The animals were perfused transcardially with phosphate buffered saline (PBS, 0.1 M, pH 7.4) followed by 4% paraformaldehyde in PBS. The brains were sagittally cut into halves for post-fixation overnight in the same fixative at 4 °C. The samples were washed in PBS and transferred to an antigen retrieval solution [10 mM sodium citrate, pH 6.0 (Ino, 2003)] for overnight incubation at 4 °C. The samples were then immersed in 300 ml of preheated (95 °C) retrieval solution for 3 min. They were immediately placed in cold 30% sucrose in PBS and incubated at 4 °C overnight. The blocks were immersed in Tissue-Tek OCT Compound (Sakura Fine Technical, Tokyo, Japan), frozen with dry ice, and stored at −80 °C. Cryosections (40 μm thick) cut frontally through the hippocampus using a sliding microtome (Leica CM3000, Leica Microsystems, Bannockburn, IL, USA) were collected sequentially into eight series in a cryoprotectant solution [ethyleneglycol: glycerol:PBS (1:1:2, v/v)] and stored at −20 °C.

Silver staining

For the staining of degenerating neurons, we prepared 8–10 sections from the short-term group [non-Tg(NS) ($n=2$), non-Tg(ST) ($n=2$), L/V-Tg(NS) ($n=2$), L/V-Tg(ST) ($n=2$)] and 12–14 sections from the long-term group [non-Tg(NS) ($n=3$), non-Tg(ST) ($n=3$), L/V-Tg(NS) ($n=3$), L/V-Tg(ST) ($n=3$)]. The mice were perfused as described above. The whole brains were post-fixed for 48 h at 4 °C. Right brain hemispheres were immersed in an embedding medium, frozen with dry ice and stored at −80 °C. Silver staining of cryostat sections was performed using an FD NeuroSilver Kit II (FD NeuroTechnologies, Ellicott City, MD, U.S.A.) according to the manufacturer's protocol to detect degenerating neurons. Sections [Bregma −1.58~−2.92 (Paxinos and Franklin, 2001)] viewed on a video monitor connected to a LEICA DM2500 microscope (×20 NA

0.40 objective) with a LEICA DFC 300-FX digital camera were used for cell counting. The degenerating cells in the dentate gyrus (DG), Cornus Ammonis 3 (CA3), retrosplenial cortex (RCtx), and piriform cortex (PCtx) were counted using the analyze particle mode of Object-Image2.15 (US National Institutes of Health and at the University of Amsterdam). The analytical process was as follows: microscopic color images (each 0.16 mm^2) were opened using the Object-Image2.15 software and through a red channel image, degenerating neurons were selected by density slice mode. The degenerating neurons were always indicated by dense silver precipitates, which appear as black grains in their somata and cells with numerous fine grains in their somata and were counted using the analyze particles mode with several optional settings (i.e. 'minimal particle size of 20 pixels,' 'label particles,' 'outline particles,' 'ignore particles touching edge,' and 'include interior holes'). The numerical density of the degenerating cells was converted to a percentage of the cell number in non-Tg(NS) mice.

Immunohistochemical analysis

Serial sections (40 μm thick) were processed for immunostaining using a primary antibody against Pax6 (Inoue et al., 2000) (anti-Pax6 rabbit antibody 63, 1:500) [non-Tg(NS) ($n=5$), non-Tg(ST) ($n=5$), L/V-Tg(NS) ($n=5$), L/V-Tg(ST) ($n=5$)], Ki-67 (anti-Ki-67 rabbit serum, 1:50;YLEM, Roma, Italy, #PRO229) [non-Tg(NS) ($n=7$), non-Tg(ST) ($n=6$), L/V-Tg(NS) ($n=7$), L/V-Tg(ST) ($n=6$)], or double-cortin (DCX) (anti-DCX guinea pig antibody, 1:3000; Chemicon, CA, USA, #AB5910) [non-Tg(NS) ($n=9$), non-Tg(ST) ($n=8$), L/V-Tg(NS) ($n=9$), L/V-Tg(ST) ($n=8$)]. Free-floating sections were treated first with PBS containing 10% methanol and 3% H_2O_2 for 30 min at room temperature and rinsed in PBS. The sections were next treated with 3% normal goat serum in PBS containing 0.1% Triton X-100 for 2 h at room temperature and incubated for 48 h in the primary antibody solution at 4 °C. Then they were incubated with biotinylated goat anti-rabbit IgG (1:5000; Vector, CA, USA, #BA-1000) for Pax6 and Ki-67 or biotinylated goat anti-guinea pig IgG (1:500; Vector #BA-7000) for DCX for 2 h at room temperature. The immunoreactions with the ABC reagent (Vector) and the ImmunoPure Methal Enhanced DAB Substrate Kit (PIERCE, Rockford, IL, USA) were done according to the manufacturer's protocol. The sections were placed onto an MAS-coated slide glass (Matsunami, Osaka, Japan, #S9443), air-dried, dehydrated with ethanol and xylene, and coverslipped with HSR solution (International Reagents Corp., Kobe, Japan).

BrdU labeling

For the labeling of mitotic cells, the mice received an intraperitoneal injection of 5-bromo-2′-deoxyuridine (BrdU, Sigma, 15 mg/ml dissolved in 0.9% NaCl, 20 μl/g body weight) at 4:30–5:00 pm and were perfused 20 h after injection [non-Tg(NS) ($n=5$), non-Tg(ST) ($n=4$), L/V-Tg(NS) ($n=5$), L/V-Tg(ST) ($n=5$)]. This high dose of BrdU (300 mg/kg) is a specific, quantitative, and nontoxic marker of dividing cells in the adult DG (Cameron and McKay, 2001). Free-floating sections (40 μm thick) were made and incubated in 2 N HCl for 30 min at 37 °C. After being rinsed in borate buffer and PBS, sections were incubated with an anti-BrdU rat monoclonal antibody (1:500, abcam, Cambridge, MA, USA, #ab6326) overnight at 4 °C and then with the secondary antibody for 2 h at room temperature. The immunoreactions with the ABC reagent and DAB were performed as described above.

Quantification and stereology

Serial sections [six sections from each animal, Bregma −1.34 to −3.08 (Paxinos and Franklin, 2001)] (Supplementary Fig. 2) of one hemisphere were taken for stereological quantification of the dentate GCL, including the Pax6-, Ki-67-, DCX-, and BrdU-positive cells in the GCL and subgranular zone (SGZ, a two-cell-thick layer in the granule cell layer, is located close to the hilus or in the lower part of the GCL). For Pax6 or Ki-67 immunostaining, toluidine blue-stained serial sections were used to determine the total volume of the GCL. DAB-stained individual sections were viewed on a video monitor connected to a Zeiss Axiophot 2 microscope (2.5× NA 0.12 objective) with a 3CCD Fuji (Fujifilm, Tokyo, Japan) digital camera. Part of the GCL was delineated by drawing a line, using the programmed tool in Adobe Photoshop7.0 (Adobe Systems Inc., San Jose, CA, USA). The total area of the GCL was measured using Object-Image2.15, and the resultant volume (pixels) was converted into micrometers. Individual cells were visualized using the same system described above (10× NA 0.45 objective), and the marker-positive cells were counted in the GCL, SGZ, and hilus. The cells were counted by an observer blinded to the genotype and the treatment status.

Statistical analyses

For every parameter, the values were first calculated separately for each animal before the means and the standard error of the mean (SEM) were determined for the groups. The number of marker-positive cells in a fixed area (cells/mm^2) was converted to the percentage of the number of marker-positive cells in the non-Tg(NS) littermates. Data are expressed as the mean values ± SEM. All statistical analyses were performed with PRISM version 5.0a (GraphPad Software, La Jolla, CA, USA). The data were analyzed by a two-way analysis of variance (ANOVA) between genotypes (non-Tg, L/V-Tg) and treatments (non-stressed, stressed) and with a Bonferroni post hoc test. When an interaction was found, multiple comparisons were performed with the Tukey–Kramer test. Values of $P<0.05$ were considered significant.

Results

Establishment of a chronic intermittent restraint stress model

We first sought to establish an effective restraint tube-based chronic stress model (Supplementary Fig. 1) that causes long-lasting structural changes in the hippocampus. By the protocol with several weeks' continuous restraint stress, it has been pointed out that mice tend to be habituated to the stressor, making it difficult to precisely examine the effects of chronic stress (Kim and Han, 2006). A previous report also indicated that chronic intermittent restraint stress (CIRS) for 2 weeks affected adult neurogenesis in the hippocampus (Rosenbrock et al., 2005). We therefore determined that CIRS is an effective protocol to verify changes in neurogenesis and introduced a resting period during the chronic restraint protocol in which we assess the effectiveness of the stressor using the reduction in body weight gain and the hypertrophy of the adrenal glands as indices.

As a result, our CIRS protocol (Fig. 1) primarily reduced the body growth rate of both non-Tg and L/V-Tg mice under chronic stress (Fig. 2A, B). When the body weight gain, which is expressed as the difference between the end and the beginning of the experiment, was subjected to a two-way ANOVA, we found out a significant effect of treatment ($F_{1,46}=393.98$, $P<0.0001$), but not a genotype effect ($F_{1,46}=1.70$, $P=0.1990$) and no interaction ($F_{1,46}=2.14$, $P=0.1507$) in the short-term experiments. The analysis also revealed a significant effect of treatment ($F_{1,8}=25.66$, $P=0.0010$), but not a genotype effect ($F_{1,8}=0.08$, $P=0.7857$) and no interaction ($F_{1,8}=0.10$, $P=0.7618$) in the long-term experiments. Additionally, the unpaired t-test [non-Tg(ST) vs. L/V-Tg(ST)] revealed that the body weight gain of the L/V-Tg mice (−11.3 ± 0.6%) was significantly reduced compared with that of the non-Tg(ST) animals (−8.6 ± 1.0%) after short-term CIRS (two-tailed, $P=0.0266$; Supplementary Table 1). Although the body growth rate at the resting period was increased in

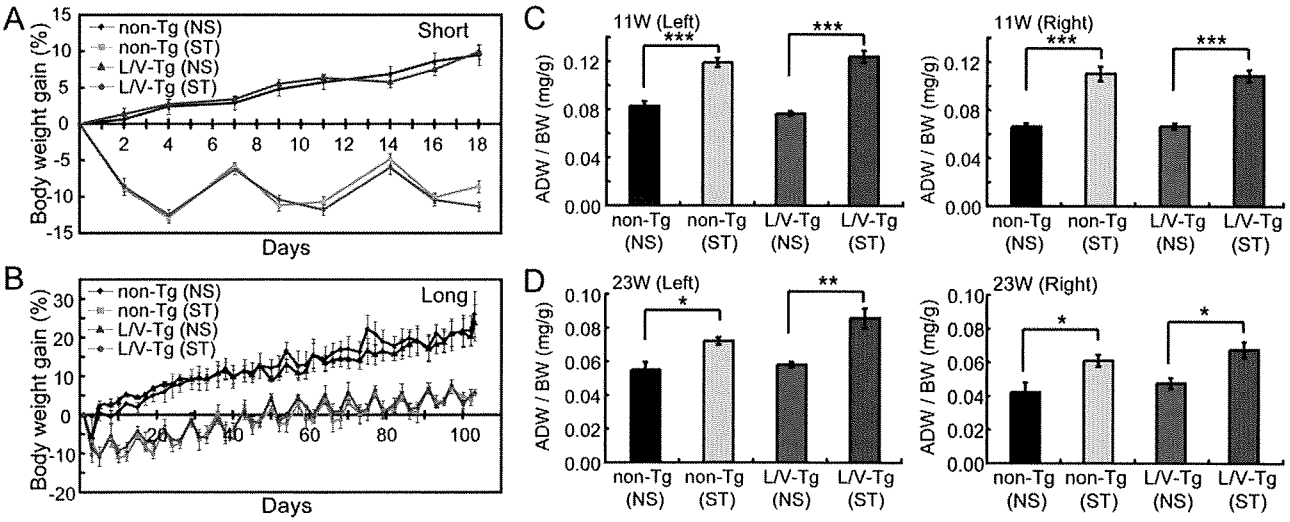

Fig. 2. Chronic intermittent restraint stress (CIRS) induces typical stress symptoms. (A, B) Changes in the body weight gain of mice in the stressed (ST) or non-stressed (NS) groups are plotted; (A) short term; (B) long term. The body weight gain 1 day before perfusion [expressed as the difference between the end and the beginning of the experiment, mean ± standard error of the mean (SEM)] is significantly reduced in stressed animals. (C, D) The left and right adrenal weights after short-term (C) or long-term (D) CIRS are significantly increased in the stressed groups. Data are expressed as the adrenal weight (mg) divided by the body weight (g) (ADW/BW, mean ± SEM). *$P<0.05$, **$P<0.01$, ***$P<0.001$ (Bonferroni, NS vs. ST). Non-Tg, transgenic negative mouse; L/V-Tg, transgenic mouse model of AD with overexpression of an FAD-type PS1; 11W, 11-week-old mice; 23W, 23-week-old mice.

every mouse, the rate of body weight change in the stressed groups showed a distinct fluctuating pattern for 15 weeks compared with that in the non-stressed groups (Fig. 2B). The weight of the right or left adrenal gland was also subjected to a two-way ANOVA, which revealed a significant effect of treatment [11-week-old mice (11W) left, $F_{1,45}=108.26$, $P<0.0001$; 11W right, $F_{1,45}=87.22$, $P<0.0001$; 23-week-old mice (23W) left, $F_{1,8}=28.17$, $P=0.0007$; 23W right, $F_{1,8}=20.57$, $P=0.0019$], but not of genotype effect (11W left, $F_{1,45}=0.24$, $P=0.6301$; 11W right, $F_{1,45}=0.02$, $P=0.8826$; 23W left, $F_{1,8}=4.17$, $P=0.0755$; 23W right, $F_{1,8}=0.57$, $P=0.4714$) and no interaction (11W left, $F_{1,45}=1.72$, $P=0.1963$; 11W right, $F_{1,45}=0.05$, $P=0.8275$; 23W left, $F_{1,8}=1.50$, $P=0.2555$; 23W right, $F_{1,8}=0.00$, $P=1.0000$) (Fig. 2C, D). Finally, the blood corticosterone levels in the groups with short-term chronic stress tended to increase (Supplementary Fig. 3). These results demonstrate that our short-term (3 weeks) and long-term (15 weeks) CIRS protocols can efficiently induce typical physical stress symptoms in mice.

CIRS increases the number of degenerating neurons

Because degenerating neurons appear in L/V-Tg mice without stress after 6 months of age (Chui et al., 1999), the obliteration of neuronal function in the neural circuit involved in cognitive function could be accelerated by the interaction of mutated genes and chronic stress. We thus examined whether stress accelerates neurodegeneration in the L/V-Tg mouse brain by means of the sliver staining: Degenerating neurons were indicated by dense silver precipitates appearing as black grains in their somata (shown by red arrowheads in Fig. 3B) and as cells with numerous fine grains in their somata (shown by red arrowheads in Fig. 3C). On the other hand, typical background signals were indicated by diluted brown particles (shown by a white arrowhead in Fig. 3B). As a result, in L/V-Tg mice degenerating neurons were selectively observed in the circuital areas that correlate with cognitive function. The number of degenerating neurons [% of non-Tg(NS)] was subjected to a two-way ANOVA, which revealed a significant effect of treatment ($F_{1,36}=9.58$, $P=0.0038$), genotype ($F_{1,36}=22.31$, $P<0.0001$), and an interaction ($F_{1,36}=7.18$, $P=0.0110$) in the DG; a significant effect of treatment ($F_{1,28}=8.88$, $P=0.0059$) and genotype ($F_{1,28}=10.13$, $P=0.0036$), but no interaction ($F_{1,28}=1.42$, $P=0.2435$) in the CA3; a significant effect of treatment ($F_{1,32}=25.68$, $P<0.0001$), but not of genotype ($F_{1,32}=2.09$, $P=0.1578$) and interaction ($F_{1,32}=2.19$, $P=0.1487$) in the RCtx; and a significant effect of genotype ($F_{1,27}=8.22$, $P=0.0079$), but not of treatment ($F_{1,27}=1.89$, $P=0.1810$) and interaction ($F_{1,27}=1.07$, $P=0.3108$) in the PCtx (Fig. 3D–G). After short-term CIRS (at 11 weeks of age), the number of degenerating neurons was significantly increased in the DG of L/V-Tg mice [Tukey–Kramer test, $P<0.0001$ vs. non-Tg(NS) and non-Tg(ST); $P<0.001$ vs. L/V-Tg(NS)] (Fig. 3D). The Bonferroni post hoc tests (NS vs. ST) revealed that CIRS increased the number of degenerating neurons in L/V-Tg mice [$P<0.05$, in the CA3 (Fig. 3E); $P<0.001$, in the RCtx (Fig. 3F)]. Especially in the hippocampus of the L/V-Tg(ST) mice, degenerating neurons were drastically increased in the SGZ of the DG, where considerable adult neurogenesis takes place (Fig. 3A). In non-Tg mice, the number of degenerating neurons was slightly increased after short-term CIRS only in the RCtx (Bonferroni test, $P<0.05$, NS vs. ST) (Fig. 3F).

After long-term CIRS (at 23 weeks of age), evidence of neurodegeneration was significantly accumulated in L/V-Tg mice compared with non-Tg mice in various brain regions, including the RCtx and the PCtx (Fig. 4D, E). The number of degenerating neurons was subjected to a two-way ANOVA. This analysis revealed a significant effect of treatment ($F_{1,52}=10.62$, $P=0.0020$), genotype ($F_{1,52}=15.45$, $P=0.0003$), but no interaction ($F_{1,52}=3.38$, $P=0.0719$) in the DG; a significant effect of treatment ($F_{1,44}=7.09$, $P=0.0108$), genotype ($F_{1,44}=19.50$, $P<0.0001$), and an interaction ($F_{1,44}=6.13$, $P=0.0172$) in the CA3; a significant effect of treatment ($F_{1,52}=6.07$,

Fig. 3. The number of degenerating neurons is increased in the brains of stressed animals (short-term). (A) Silver-stained sections of mice exposed to short-term chronic intermittent restraint stress (CIRS) (ST) or left untreated (NS). Scale bar, 100 μm. (B, C) High power pictures of degenerating neurons in the dentate gyrus (DG) (B) and piriform cortex (PCtx) (C) of L/V-Tg(ST) mice (corresponding to the insets in panel A, scale bar, 10 μm). Degenerating neurons are indicated by red arrowheads (B, C); typical background signal is indicated by a white arrowhead (B). (D–G) Graphs indicate the number of degenerating neurons [expressed as % of non-Tg(NS), mean ± SEM] in the DG (D), Cornus Ammonis 3 (CA3) (E), retrosplenial cortex (RCtx) (F), and PCtx (G). Statistical significance; DG [Tukey–Kramer test, ***$P<0.0001$ vs. non-Tg(NS); ###$P<0.0001$ vs. non-Tg(ST); @@$P<0.001$ vs. L/V-Tg (NS)] (D); CA3 (Bonferroni, NS vs. ST, @$P<0.05$) (E); RCtx (Bonferroni, NS vs. ST, #$P<0.05$; @@$P<0.001$) (F). Note that most degenerating neurons in the DG of L/V-Tg(ST) mice are located in the SGZ. Non-Tg, transgenic negative mouse; L/V-Tg, transgenic mouse model of AD with overexpression of an FAD-type PS1; 11W, 11-week-old mice.

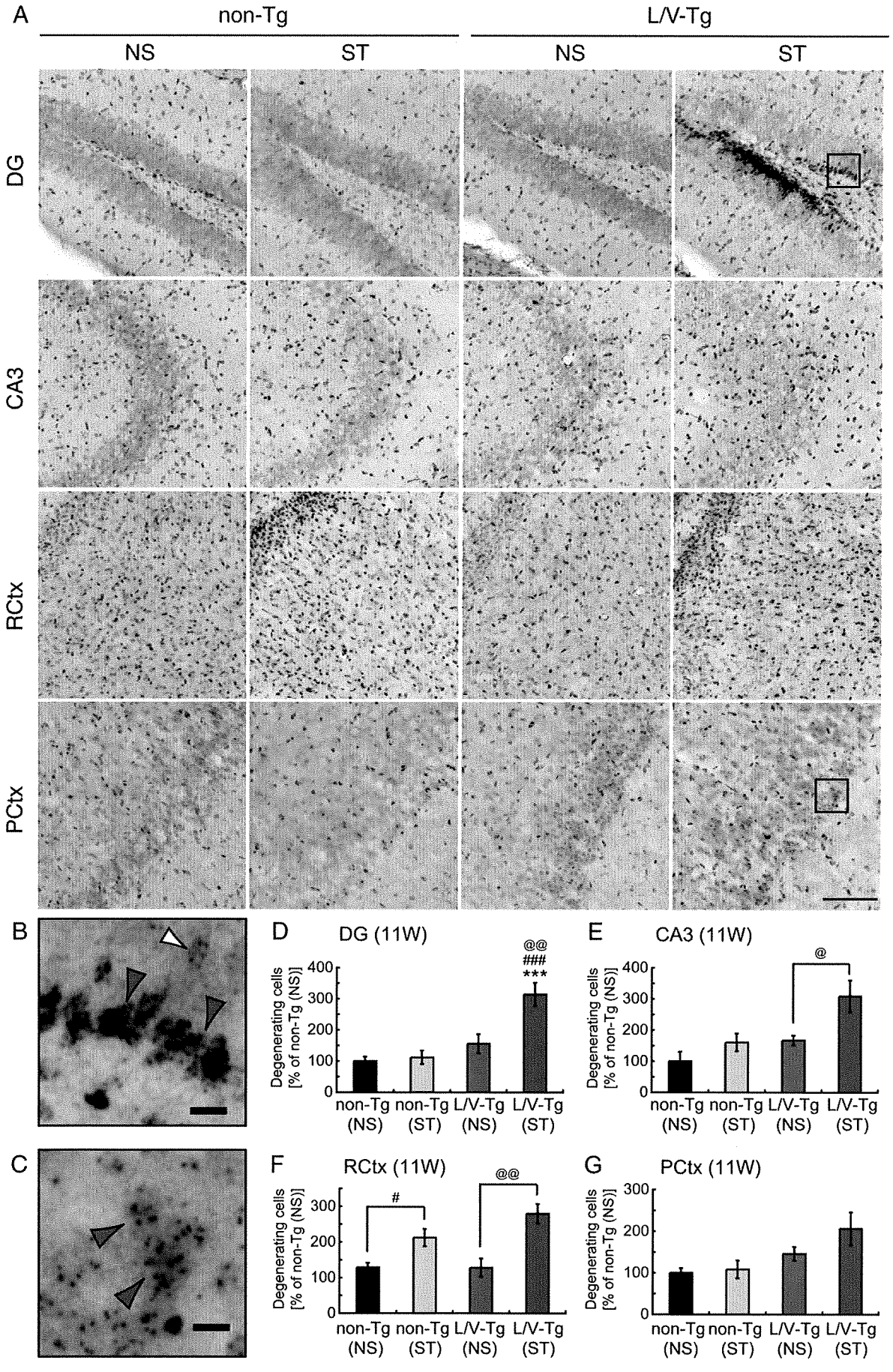
A
non-Tg
L/V-Tg
NS
ST
NS
ST
DG
CA3
RCtx
PCtx
B
C
D
DG (11W)
@@
###
***
Degenerating cells [% of non-Tg (NS)]
400
300
200
100
0
non-Tg (NS)
non-Tg (ST)
L/V-Tg (NS)
L/V-Tg (ST)
E
CA3 (11W)
@
F
RCtx (11W)
#
@@
G
PCtx (11W)

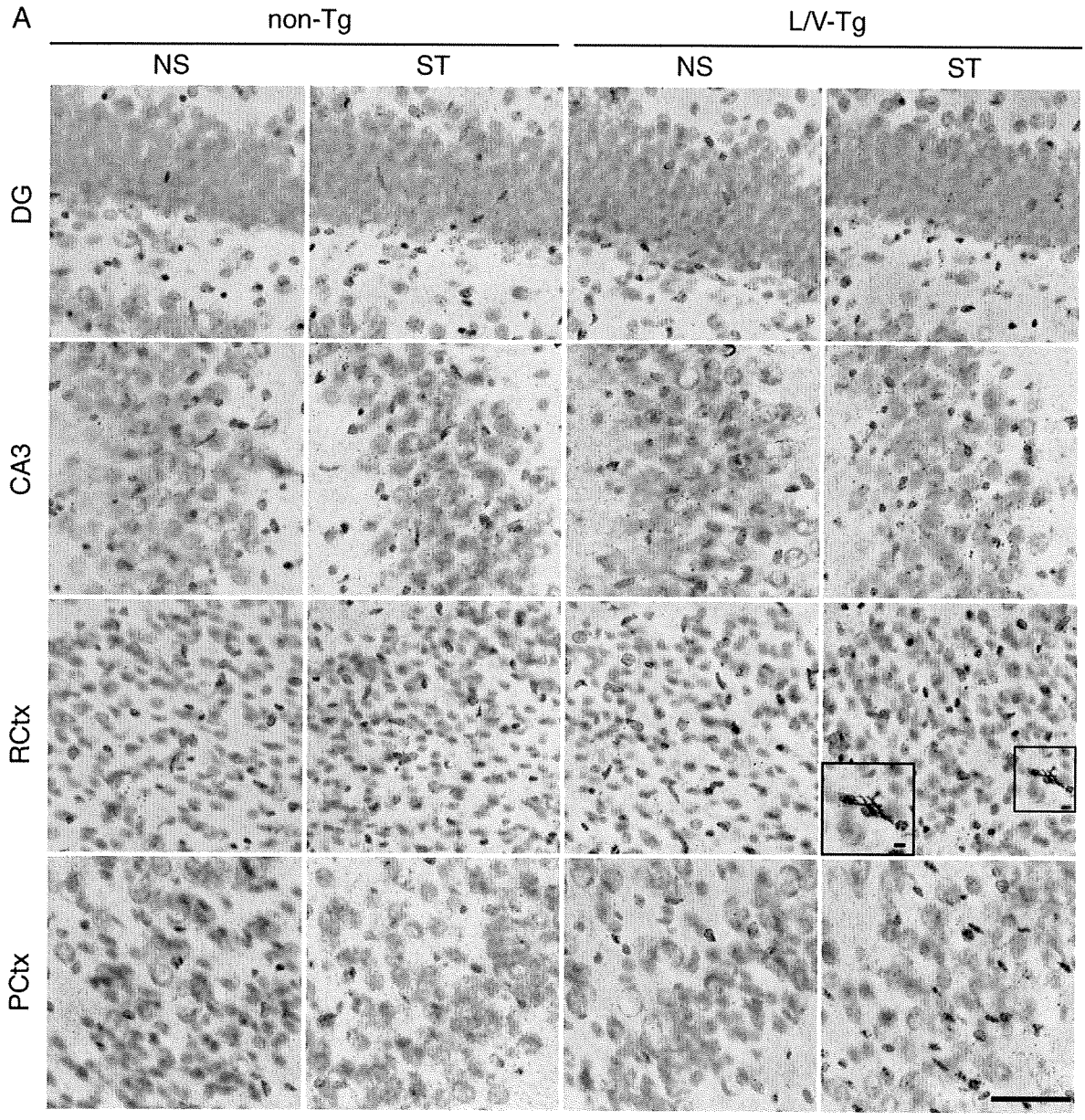
A
non-Tg
L/V-Tg
NS
ST
NS
ST
DG
CA3
RCtx
PCtx
B
DG (23W)
@@
Degenerating cells [% of non-Tg (NS)]
250
200
150
100
50
0
non-Tg (NS)
non-Tg (ST)
L/V-Tg (NS)
L/V-Tg (ST)
C
CA3 (23W)
@@
###
***
300
200
100
0
D
RCtx (23W)
#
400
300
200
100
0
E
PCtx (23W)
400
300
200
100
0

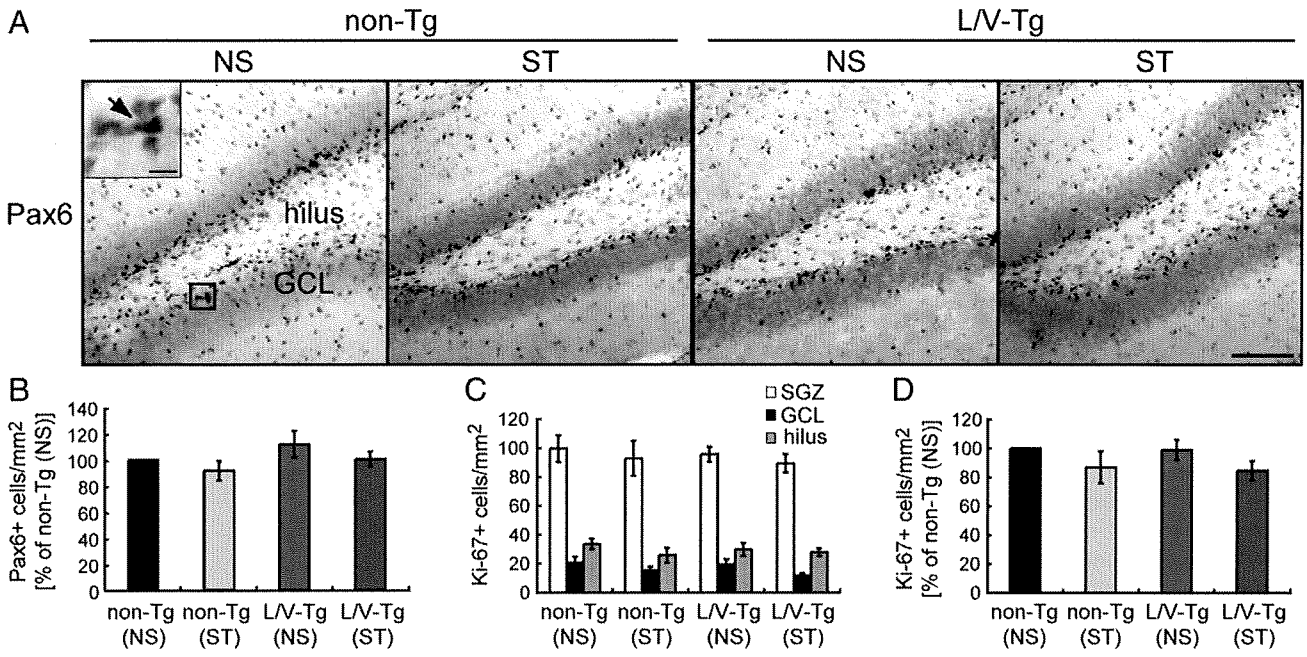

Fig. 5. Short-term chronic intermittent restraint stress (CIRS) slightly affects the number of granule neuron precursors and proliferating cells in the dentate gyrus. (A) Representative immunostaining of Pax6. Scale bar, 50 μm. Inset shows boxed region with a higher magnification (scale bar, 10 μm). An arrow indicates a Pax6+ cell. (B) The number of Pax6+ cells in the subgranular zone (SGZ) [mean ± SEM, % of non-Tg(NS)] tended to decrease in stressed (ST) animals. (C) The number of Ki-67+ cells in each hippocampal region [SGZ, hilus, and granule cell layer (GCL)]. Most Ki-67+ cells are observed in the SGZ, with considerable numbers localized to the hilar region and a few in the GCL. (D) The number of Ki-67+ cells in the GCL and SGZ is slightly decreased to a similar extent in non-Tg and L/V-Tg mice [mean ± SEM, % of non-Tg(NS)]. Non-Tg, transgenic negative mouse; L/V-Tg, transgenic mouse model of AD with overexpression of an FAD-type PS1.

$P=0.0171$) and genotype ($F_{1,52}=8.81$, $P=0.0045$), but no interaction ($F_{1,52}=1.04$, $P=0.3117$) in the RCtx; and a significant effect of genotype ($F_{1,52}=8.19$, $P=0.0061$), but not of treatment ($F_{1,52}=2.45$, $P=0.1237$) and interaction ($F_{1,52}=0.87$, $P=0.3560$) in the PCtx (Fig. 4B–E). The Bonferroni post hoc test (NS vs. ST) found that long-term CIRS significantly increased the number of degenerating cells in L/V-Tg mice [$P<0.01$, in the DG (Fig. 4B); $P<0.05$, in the RCtx (Fig. 4D)]. Multiple comparisons with the Tukey–Kramer test found a significant increase in the number of degenerating neurons in the CA3 of the L/V-Tg(ST) mice [$P<0.0001$ vs. non-Tg(NS) and non-Tg(ST); $P<0.001$ vs. L/V-Tg(NS)] (Fig. 4C).

CIRS with pathogenic PS1 slightly affects the granule neuron precursors and proliferating cells

In stressed L/V-Tg mice, the number of degenerating neurons was significantly increased in the SGZ, where adult neurogenesis occurs. To examine the effect of stress with or without pathogenic PS1 on hippocampal neurogenesis, we next evaluated the number of Pax6+ in the hippocampus of L/V-Tg and non-Tg mice using our short-term CIRS protocol. Adult neurogenesis is an individualized, entire multi-step process but not a population event (Kempermann et al., 2004). Pax6, an essential transcription factor required for the production and maintenance of neural progenitor cells (Maekawa et al., 2005), is expressed in lineage-determined neuronal progenitors, differentiating granule neurons and bipotential (neural) precursor cells, and is strongly down-regulated during granule neuron differentiation (Nacher et al., 2005). In the adult hippocampal DG, proliferating granule neuron precursors that express GFAP and nestin molecules are always Pax6+ (Hevner et al., 2006; Maekawa et al., 2005; Nacher et al., 2005). Thus, Pax6 recently has been used as a suitable marker for newly generated cells (Osumi et al., 2008; von Bohlen Und Halbach, 2007; Winner et al., 2009). Whereas a small subpopulation of hilar mature neurons and certain astrocytes of the adult hippocampus express Pax6, Pax6+ cells in the SGZ are mostly granule neuron precursors (Nacher et al., 2005). Therefore, to evaluate the number of granule neuron precursors, we counted the cells expressing Pax6 localized in the SGZ where considerable new cell production occurs. We found that most Pax6+ cells were in the SGZ (Fig. 5A) and the number of these cells [% of non-Tg(NS)] tended to decrease in non-Tg (ST) and L/V-Tg(ST) mice (Fig. 5B). Yet, a two-way ANOVA revealed no significant effect of treatment ($F_{1,16}=2.04$, $P=0.1720$), genotype ($F_{1,16}=2.31$, $P=0.1479$), or interaction ($F_{1,16}=0.05$, $P=0.8203$). Consequently, we found that neither 3 weeks of CIRS (short-term) nor the PS1(L286V) genotype greatly affects the number of granule neuron precursors in the SGZ.

Granule neuron precursors are born in the SGZ and a neural precursor produces a bipotential neural cell and a lineage-determined neuronal cell through asymmetric division (Kempermann et al., 2004). We also measured the number of Ki-67+ cells per GCL to evaluate the proliferating cells. Ki-67 is present only in proliferating cells during G1, S, G2, and M, but not in the G0 phase of the cell cycle (Brown and Gatter, 1990; Kee et al., 2002). The number of Ki-67+ cells was subjected to a two-way ANOVA, which showed no significant effect of genotype [$F_{1,22}=0.18$, $P=0.6758$ (SGZ); $F_{1,22}=0.03$, $P=0.8705$ (hilus); $F_{1,22}=0.54$, $P=0.4710$ (GCL)], treatment [$F_{1,22}=0.61$, $P=0.4442$ (SGZ); $F_{1,22}=1.32$, $P=0.2631$ (hilus); $F_{1,22}=3.63$, $P=0.0700$ (GCL)], or interaction [$F_{1,22}=0.00$, $P=0.9901$ (SGZ); $F_{1,22}=0.60$, $P=0.4481$ (hilus); $F_{1,22}=0.12$, $P=0.7277$ (GCL)] (Fig. 5C). The percentage of Ki-67+ cells in the GCL and SGZ also

Fig. 4. The number of degenerating neurons is increased in the brains of stressed animals (long-term). (A) Silver-stained sections of mice exposed to chronic intermittent restraint stress (CIRS) (ST) or left untreated (NS). Scale bar, 100 μm. Inset shows boxed regions with higher magnification (scale bar, 10 μm). (B–E) Graphs indicate the number of degenerating neurons [expressed as % of non-Tg(NS), mean ± SEM] in the dentate gyrus (DG) (B), Cornus Ammonis 3 (CA3) (C), retrosplenial cortex (RCtx) (D), and piriform cortex (PCtx) (E). Statistical significance; DG (Bonferroni, NS vs. ST, @@$P<0.01$) (B); CA3 [Tukey–Kramer test, ***$P<0.0001$ vs. non-Tg(NS); ###$P<0.0001$ vs. non-Tg(ST); @@$P<0.001$ vs. L/V-Tg(NS)] (C); RCtx (Bonferroni, NS vs. ST, #$P<0.05$) (D). Non-Tg, transgenic negative mouse; L/V-Tg, transgenic mouse model of AD with overexpression of an FAD-type PS1; 23W, 23-week-old mice.

showed no significant effect of genotype ($F_{1,22}=0.05$, $P=0.8247$) or treatment ($F_{1,22}=3.84$, $P=0.0629$) or an interaction ($F_{1,22}=0.01$, $P=0.9205$). As a result, 3 weeks of CIRS slightly decreased the number of Ki-67+ proliferating cells in the SGZ, hilus, and GCL to a similar extent in non-Tg and L/V-Tg mice (Fig. 5C, D). In short, we confirmed that short-term CIRS primarily decreased the production of granule neuron precursors and the number of proliferating cells in the GCL and SGZ, yet the effect did not show significant differences between non-Tg and L/V-Tg backgrounds.

The impact of CIRS on newly synthesized cells lasts longer in Tg than in Non-Tg

In order to quantify the rate of neural production in the GCL and SGZ after stress exposure, we counted the newly synthesized cells by a single intraperitoneal injection of BrdU 20 h before perfusion. Unlike the measurement of the Pax6+ granule neuron precursors that integrates all of the marker-positive cells produced during the whole experimental (stressed/non-stressed) period, this BrdU labeling protocol can estimate only those cells newly synthesized within a day after stress cessation. When using Ki-67 to quantify the cell proliferation, newly generated cells that exit the cell cycle and enter their maturation process are not detected. BrdU is incorporated in cells at the S-phase, allowing us to detect both mitotic cells (Type-1, Type-2a, 2b, Type-3) and postmitotic cells (including late Type-3) in the hippocampal DG [the classification of the cellular stage in neurogenesis was performed in accordance with the review by Kempermann (Kempermann et al., 2004)] by immunohistochemical analyses using an anti-BrdU antibody. Actually, in adult hippocampal neurogenesis of mice, one can find a considerable number of cells labeled for both BrdU and NeuN (a post-mitotic, neuronal cell marker) even 1 day after a single injection of BrdU (Brandt et al., 2003). The number of BrdU+ cells in the GCL and SGZ [% of non-Tg(NS)] was subjected to a two-way ANOVA, and this analysis did show a significant effect of treatment ($F_{1,15}=24.12$, $P=0.0002$), but no effect of genotype ($F_{1,15}=2.06$, $P=0.1716$) and interaction ($F_{1,15}=1.78$, $P=0.2026$). Bonferroni *post hoc* tests (NS vs. ST) revealed that after CIRS, the number of BrdU+ cells was significantly reduced in L/V-Tg mice ($P<0.001$) [63 ± 7% of BrdU + cells in non-Tg(NS), Fig. 6A, B] but was not significantly decreased in non-Tg mice ($P>0.05$) [79 ± 9% of BrdU+ cells in non-Tg(NS), Fig. 6A, B]. This trend was almost parallel with the pattern in the body-weight-gain reductions (Supplementary Table 1). These results indicate that the impact of stress on newly synthesized cells in L/V-Tg mice lasted longer than that in non-Tg mice.

DCX+ neuronal progenitor cells increased after CIRS only in Tg

Although the significant reduction in the number of BrdU+ newly synthesized cells at 20 h after stress in L/V-Tg mice was apparent, the number of Pax6+ granule neuron precursors in the SGZ and Ki-67+ proliferating cells in the GCL and SGZ did not significantly decrease during the short-term CIRS. In hippocampal neurogenesis, a dividing precursor cell gives rise to daughter cells, which migrate away from the site of division and start to differentiate into neurons (Kempermann et al., 2004). We therefore evaluated the effect of short-term CIRS on the neuronal progenitor cells in the GCL and SGZ using the microtubule-associated protein doublecortin (DCX) as a marker. DCX is normally retained in cells within areas of continuous neurogenesis and expressed in mitotic and postmitotic cells (Brown et al., 2003; Couillard-Despres et al., 2005; Rao and Shetty, 2004), namely, proliferative nestin-positive neuronal progenitor cells (Type-2b), nestin-negative neuronal progenitor cells (Type-3), and postmitotic immature neurons that retain the vertical morphology with a rounded or slightly triangular nucleus and a clearly visible apical dendrite (late Type-3) (Kempermann et al., 2004). As the

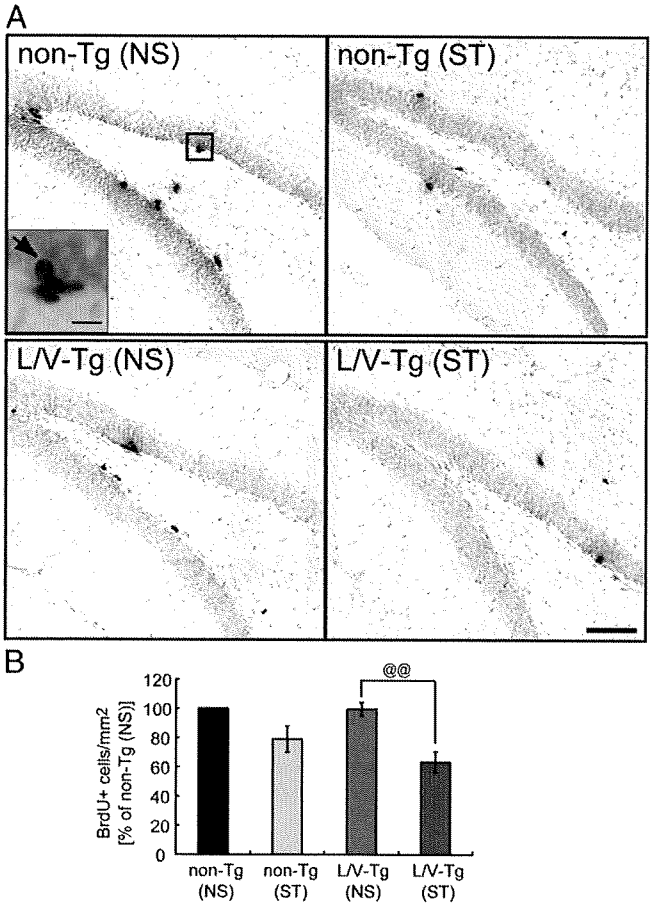

Fig. 6. The impact of chronic intermittent restraint stress (CIRS) on newly synthesized cells in the granule cell layer (GCL) and the subgranular zone (SGZ) lasts longer in L/V-Tg mice than in non-Tg mice. (A) Representative immunostaining of 5-bromo-2′-deoxyuridine (BrdU)+ cells. Scale bar, 50 μm. Inset shows boxed region with a higher magnification (scale bar, 10 μm). An arrow indicates a BrdU+ cell. (B) After CIRS, the number of BrdU+ cells in the GCL and SGZ [mean ± SEM, % of non-Tg(NS)] is significantly reduced in L/V-Tg mice (Bonferroni, NS vs. ST, @@$P<0.001$) but is not significantly decreased in non-Tg mice. Non-Tg, transgenic negative mouse; L/V-Tg, transgenic mouse model of AD with overexpression of an FAD-type PS1; NS, non-stressed control mice; ST, stressed mice.

newly generated cells began expressing mature neuronal markers, DCX immunoreactivity decreased sharply below the level of detection and remained undetectable thereafter (Brown et al., 2003; Couillard-Despres et al., 2005; Rao and Shetty, 2004). The number of DCX+ cells in the GCL and SGZ [% of non-Tg(NS)] was subjected to a two-way ANOVA, and this analysis showed a significant effect of treatment ($F_{1,30}=5.48$, $P=0.0261$) and an interaction ($F_{1,30}=23.37$, $P<0.0001$), but no effect of genotype ($F_{1,30}=1.76$, $P=0.1943$). Tukey-Kramer post hoc tests revealed significant differences in the number of DCX+ progenitor cells in the GCL and SGZ. In stressed non-Tg mice, the number of DCX+ cells significantly reduced [$P<0.0001$ vs. non-Tg(NS)] (Fig. 7A, B). This is in agreement with the trends observed for the Pax6+, Ki-67+, and BrdU+ cells. On the other hand, in L/V-Tg mice, the number of DCX+ cells was significantly reduced without stress [78 ± 2 % of DCX+ cells in non-Tg(NS); $P<0.0001$ vs. non-Tg(NS), Fig. 7B]. Unexpectedly, in L/V-Tg mice, the number of DCX+ neuronal progenitors was significantly increased by short-term CIRS [12 % increase compared with non-stressed L/V-Tg; $P<0.001$ vs. L/V-Tg(NS), Fig. 7B]. Equivalent data were obtained from confocal laser scanning microscopic analyses of the doublecortin (DCX)+ neuronal progenitor cells in the GCL and SGZ (Supplementary Fig. 4). Additionally, in the stressed L/V-Tg mice, the percentage of DCX+ cells that possessed long neurites (late

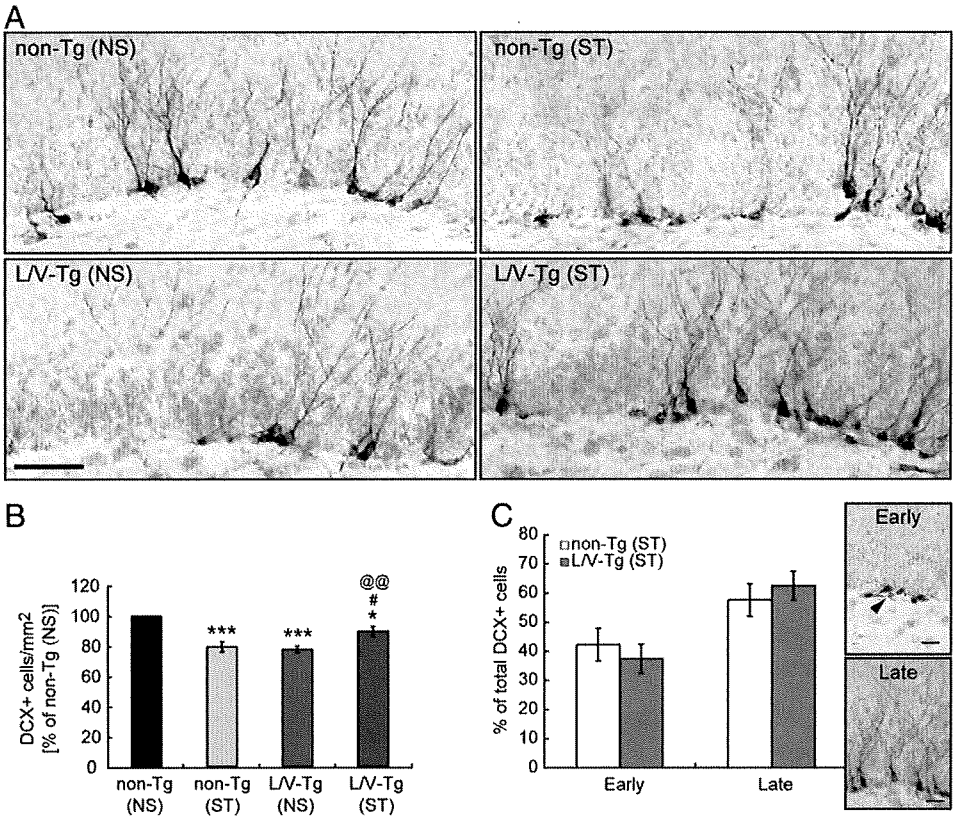

Fig. 7. Neuronal progenitor cells in the granule cell layer (GCL) and the subgranular zone (SGZ) increase after chronic intermittent restraint stress (CIRS) only in Tg. (A) Representative immunostaining of the doublecortin (DCX)+ neuronal progenitor cells in the GCL and SGZ. Scale bar, 50 μm. (B) The DCX+ cells in the GCL and SGZ [mean ± SEM, % of non-Tg(NS)] are significantly reduced in non-stressed L/V-Tg mice and are increased in stressed L/V-Tg mice. *P<0.05, ***P<0.0001 vs. non-Tg(NS); #P<0.05 vs. non-Tg(ST); @@P<0.001 vs. L/V-Tg(NS) (Tukey–Kramer test). (C) The percentage of DCX+ cells that possessed short neurites (Early, early progenitor cells) or long neurites (Late, late progenitor cells) in non-Tg(ST) and L/V-Tg(ST) mice (mean ± SEM). Scale bar, 50 μm. DCX+ late progenitor cells are modestly increased in L/V-Tg(ST) mice compared with non-Tg(ST) mice. Non-Tg, transgenic negative mouse; L/V-Tg, transgenic mouse model of AD with overexpression of an FAD-type PS1; NS, non-stressed control mice; ST, stressed mice.

progenitor cells) was modestly increased over that of non-Tg mice, whereas early progenitor cells tended to decrease compared with that of non-Tg mice (Fig. 7C).

Discussion

Our study indicates how gene–environment interaction affects adult neurogenesis in the hippocampal DG and deteriorates selective neurodegeneration in the neuronal circuit involved in cognitive function. We speculate that, in genetically predisposed animals, accumulated effects of subtle daily stresses such as metabolic oxidation may cause neurodegeneration, even in the absence of environmental stress.

Cellular and molecular machineries that accelerate neurodegeneration by chronic stress

Neurodegeneration in stressed L/V-Tg mice was more severe than in stressed non-Tg mice (Fig. 3). This might be due to increased vulnerability at the cellular or system levels, which is supported by our observation of abnormal calcium homeostasis in primary cultured hippocampal neurons prepared from neonatal L/V-Tg mice (data not shown). A previous report indicated that the PS1(L286V) mutation lowers the threshold to neurotoxicity through the disruption of calcium homeostasis and increased free radical production (Grilli et al., 2000; Guo et al., 1997). While structural changes after stress are often found in the CA3 (Conrad, 2006), we found that neurodegeneration in the stressed L/V-Tg mice was most prominent in the SGZ of the DG, where adult neurogenesis occurs. Because PS1 plays a role in neurogenesis both during development and in the adult (Wen et al., 2002), neurogenesis in the SGZ could be affected by chronic stress more than that in non-Tg mice.

In L/V-Tg mice, the number of DCX+ neuronal progenitors in the GCL and SGZ was significantly reduced without stress (Fig. 7A, B). This is in accord with recent evidence demonstrating that an FAD-related homozygous PS1 P264L mutation resulted in decreased numbers of DCX+ cells in the GCL (Zhang et al., 2007). On the other hand, the number of DCX+ cells in the GCL was significantly increased by short-term CIRS (Fig. 7A, B), which is consistent with the observation that the number of DCX+ cells in the hippocampal GCL increases in a senile cohort of AD patients (Jin et al., 2004). Another recent publication shows that increased proliferating cells in the presenile AD hippocampus are mostly accounted for by glial and vascular-associated changes, but not by neurogenesis (Boekhoorn et al., 2006). These contradictions can be attributed to multiple factors, such as different phases of AD progression, animal models, methodologies, and analytical tools (Kuhn et al., 2007). In our study, both decreased and increased states of DCX+ cells were driven in the L/V-Tg mice using the chronic stress model. These mice would therefore contribute to unravelling the aberrant neurogenic/nonneurogenic mechanisms that are part of the pathological events of neurodegenerative diseases.

Despite increased numbers of DCX+ cells in the GCL of AD patients (Jin et al., 2004) and short-term chronically stressed L/V-Tg mice, progressive neurodegeneration was still observed after long-term CIRS, implicating that the repair capacity of the DCX+ cells in the GCL is limited. Notably, the number of BrdU+ newly synthesized cells was significantly reduced in the GCL and SGZ (Fig. 6A, B). Considering the fact that BrdU+ cells contain both neural and neuronal fate cells (Maekawa et al., 2005), together with the observation that production of Pax6+ granule neuron precursors in the SGZ reached a similar

extent in stressed non-Tg and L/V-Tg mice, cells with a neuronal fate might preferentially be reduced in 20 h after CIRS. In stressed L/V-Tg mice, percentage of postmitotic DCX+ cells possessing longer neurites (late Type-3) was modestly increased compared with that in non-Tg (ST) mice, whereas the number of mitotic DCX+ cells (Type-2b and early Type-3) tended to decrease compared with that of non-Tg(ST) mice (Fig. 7C). This indicates that numerous DCX+ neuronal progenitor cells observed in the GCL and SGZ of stressed L/V-Tg mice were late-stage (posmitotic late Type-3), rather than early-stage (mitotic Type-2b and Type-3), in neuronal maturation. Collectively, these data suggest that an interaction between pathogenic PS1 and CIRS does affect neurogenesis during postmitotic neuronal cell maturation. We reasoned that the elevated number of DCX+ cells in the GCL and SGZ of stressed L/V-Tg mice was derived from an accumulation of immature neuronal progenitor cells rather than a replenishment of granule cells. A recent report indicated that DCX molecule supports dendritic arborization (Cohen et al., 2008). Given that DCX+ cells were accumulated in the GCL of stressed L/V-Tg mice, abnormal DCX degradation and consequent excessive stabilization of microtubules by DCX could in part explain the retardation of neuronal maturation and the resultant neurodegeneration. PS1 mutations might synergistically affect the expression, processing, or trafficking of molecules essential to neuronal maturation, such as Wnts, BDNF, and Trk receptors (Naruse et al., 1998), although further molecular–cellular assessment would be needed.

From a therapeutic point of view, it is necessary to elucidate the detailed molecular machinery that perturbs granule cell maturation and neurodegeneration in the hippocampal DG. The ability to recover from stress-related impaired neurogenesis, which was shown in wild-type adult rats (Heine et al., 2004), would be unbalanced presumably by the vulnerability derived from the mutated gene–chronic stress interaction in stressed L/V-Tg mice. For instance, under the stressed condition, apoptosis machinery is not available in L/V-Tg mice to actively eliminate those cells in abnormal neuronal differentiation, resulting in an accumulation of ill-balanced neurodegenerative cells in the hippocampus, even at the younger stages. This is partly supported by our observation that the number of TUNEL-positive apoptotic cells in the GCL did not significantly fluctuate between L/V-Tg and wild-type mice with CIRS (Supplementary Fig. 5), and the phenotype might further be strengthened by the fact that the number of newly synthesized cells assessed by BrdU was 33% decreased in L/V-Tg(ST) mice (Fig. 6). A non-cell autonomous microenvironmental niche induced by FAD-linked PS1 variants could be additionally responsible for the impaired neurogenesis and neurodegeneration (Choi et al., 2008).

Conclusions

Our results suggest that, in individuals predisposed to genetic mutations for AD, stress accelerates the inhibition of neuronal maturation, thereby enhancing neurodegenerative vulnerability that depends on mutated gene–environment interaction. Chronically stressed L/V-Tg mice could be useful animal models to elucidate the key molecular machinery and therapeutic targets for AD. Our experimental strategy using controlled stress should provide insights into the pathogenic mechanisms of AD as well as other neurodegenerative diseases.

Acknowledgments

We thank Drs. S. Kohsaka and M. Hoshino for their help, Ms. T. Kohno and J. Asami for technical assistance and all other members of the Shindan, DDND and DVDR lab for fruitful discussions. We also thank Drs. H. Kumanogoh, R. Setsuie, K. Zushida, T. Maruoka, M. Yokosuka, K. Yuyama, T. Kikusui, and K. Moriya for providing useful information. This work was supported by a Grant-in-Aid for Young Scientists (B) (#18790607; #21790639) to S.K., grants from Research Foundation ITSUU Laboratory and Takeda Science Foundation to T.I., and the Program for Promotion of Fundamental Studies in Health Sciences of the National Institute of Biomedical Innovation (05-32) to S. N., K. W. and T. I.

Appendix A. Supplementary data

Supplementary data associated with this article can be found, in the online version, at doi:10.1016/j.expneurol.2009.10.020.

References

Boekhoorn, K., Joels, M., Lucassen, P.J., 2006. Increased proliferation reflects glial and vascular-associated changes, but not neurogenesis in the presenile Alzheimer hippocampus. Neurobiol. Dis. 24, 1–14.
Brandt, M.D., Jessberger, S., Steiner, B., Kronenberg, G., Reuter, K., Bick-Sander, A., von der Behrens, W., Kempermann, G., 2003. Transient calretinin expression defines early postmitotic step of neuronal differentiation in adult hippocampal neurogenesis of mice. Mol. Cell. Neurosci. 24, 603–613.
Brown, D.C., Gatter, K.C., 1990. Monoclonal antibody Ki-67: its use in histopathology. Histopathology 17, 489–503.
Brown, J.P., Couillard-Després, S., Cooper-Kuhn, C.M., Winkler, J., Aigner, L., Kuhn, H.G., 2003. Transient expression of doublecortin during adult neurogenesis. J. Comp. Neurol. 467, 1–10.
Bruel-Jungerman, E., Laroche, S., Rampon, C., 2005. New neurons in the dentate gyrus are involved in the expression of enhanced long-term memory following environmental enrichment. Eur. J. Neurosci. 21, 513–521.
Buckner, R.L., 2004. Memory and executive function in aging and AD: multiple factors that cause decline and reserve factors that compensate. Neuron 44, 195–208.
Cameron, H.A., McKay, R.D., 2001. Adult neurogenesis produces a large pool of new granule cells in the dentate gyrus. J. Comp. Neurol. 435, 406–417.
Choi, S.H., Veeraraghavalu, K., Lazarov, O., Marler, S., Ransohoff, R.M., Ramirez, J.M., Sisodia, S.S., 2008. Non-cell-autonomous effects of presenilin 1 variants on enrichment-mediated hippocampal progenitor cell proliferation and differentiation. Neuron 59, 568–580.
Chui, D.H., Tanahashi, H., Ozawa, K., Ikeda, S., Checler, F., Ueda, O., Suzuki, H., Araki, W., Inoue, H., Shirotani, K., Takahashi, K., Gallyas, F., Tabira, T., 1999. Transgenic mice with Alzheimer presenilin 1 mutations show accelerated neurodegeneration without amyloid plaque formation. Nat. Med. 5, 560–564.
Cohen, D., Segal, M., Reiner, O., 2008. Doublecortin supports the development of dendritic arbors in primary hippocampal neurons. Dev. Neurosci. 30, 187–199.
Conrad, C.D., 2006. What is the functional significance of chronic stress-induced CA3 dendritic retraction within the hippocampus? Behav. Cogn. Neurosci. Rev. 5, 41–60.
Couillard-Despres, S., Winner, B., Schaubeck, S., Aigner, R., Vroemen, M., Weidner, N., Bogdahn, U., Winkler, J., Kuhn, H.G., Aigner, L., 2005. Doublecortin expression levels in adult brain reflect neurogenesis. Eur. J. Neurosci. 21, 1–14.
Drapeau, E., Mayo, W., Aurousseau, C., Le Moal, M., Piazza, P.V., Abrous, D.N., 2003. Spatial memory performances of aged rats in the water maze predict levels of hippocampal neurogenesis. Proc. Natl. Acad. Sci. U. S. A. 100, 14385–14390.
Golde, T.E., Eckman, C.B., Younkin, S.G., 2000. Biochemical detection of Abeta isoforms: implications for pathogenesis, diagnosis, and treatment of Alzheimer's disease. Biochim. Biophys. Acta 1502, 172–187.
Gould, E., Tanapat, P., 1999. Stress and hippocampal neurogenesis. Biol. Psychiatry 46, 1472–1479.
Gould, E., Beylin, A., Tanapat, P., Reeves, A., Shors, T.J., 1999. Learning enhances adult neurogenesis in the hippocampal formation. Nat. Neurosci. 2, 260–265.
Grilli, M., Diodato, E., Lozza, G., Brusa, R., Casarini, M., Uberti, D., Rozmahel, R., Westaway, D., St George-Hyslop, P., Memo, M., Ongini, E., 2000. Presenilin-1 regulates the neuronal threshold to excitotoxicity both physiologically and pathologically. Proc. Natl. Acad. Sci. U. S. A. 97, 12822–12827.
Guo, Q., Sopher, B.L., Furukawa, K., Pham, D.G., Robinson, N., Martin, G.M., Mattson, M.P., 1997. Alzheimer's presenilin mutation sensitizes neural cells to apoptosis induced by trophic factor withdrawal and amyloid beta-peptide: involvement of calcium and oxyradicals. J. Neurosci. 17, 4212–4222.
Heine, V.M., Maslam, S., Zareno, J., Joëls, M., Lucassen, P.J., 2004. Suppressed proliferation and apoptotic changes in the rat dentate gyrus after acute and chronic stress are reversible. Eur. J. Neurosci. 19, 131–144.
Hevner, R.F., Hodge, R.D., Daza, R.A., Englund, C., 2006. Transcription factors in glutamatergic neurogenesis: conserved programs in neocortex, cerebellum, and adult hippocampus. Neurosci. Res. 55, 223–233.
Imayoshi, I., Sakamoto, M., Ohtsuka, T., Takao, K., Miyakawa, T., Yamaguchi, M., Mori, K., Ikeda, T., Itohara, S., Kageyama, R., 2008. Roles of continuous neurogenesis in the structural and functional integrity of the adult forebrain. Nat. Neurosci. 11, 1153–1161.
Ino, H., 2003. Antigen retrieval by heating en bloc for pre-fixed frozen material. J. Histochem. Cytochem. 51, 995–1003.
Inoue, T., Nakamura, S., Osumi, N., 2000. Fate mapping of the mouse prosencephalic neural plate. Dev. Biol. 219, 373–383.
Jack Jr., C.R., Petersen, R.C., O'Brien, P.C., Tangalos, E.G., 1992. MR-based hippocampal volumetry in the diagnosis of Alzheimer's disease. Neurology 42, 183–188.
Jeong, Y.H., Park, C.H., Yoo, J., Shin, K.Y., Ahn, S.M., Kim, H.S., Lee, S.H., Emson, P.C., Suh, Y.H., 2006. Chronic stress accelerates learning and memory impairments and increases

amyloid deposition in APPV717I-CT100 transgenic mice, an Alzheimer's disease model. FASEB J. 20, 729–731.
Jin, K., Peel, A.L., Mao, X.O., Xie, L., Cottrell, B.A., Henshall, D.C., Greenberg, D.A., 2004. Increased hippocampal neurogenesis in Alzheimer's disease. Proc. Natl. Acad. Sci. U. S. A. 101, 343–347.
Kee, N., Sivalingam, S., Boonstra, R., Wojtowicz, J.M., 2002. The utility of Ki-67 and BrdU as proliferative markers of adult neurogenesis. J. Neurosci. Methods 115, 97–105.
Kempermann, G., Gage, F.H., 2002. Genetic determinants of adult hippocampal neurogenesis correlate with acquisition, but not probe trial performance, in the water maze task. Eur. J. Neurosci. 16, 129–136.
Kempermann, G., Jessberger, S., Steiner, B., Kronenberg, G., 2004. Milestones of neuronal development in the adult hippocampus. Trends Neurosci. 27, 447–452.
Killiany, R.J., Moss, M.B., Albert, M.S., Sandor, T., Tieman, J., Jolesz, F., 1993. Temporal lobe regions on magnetic resonance imaging identify patients with early Alzheimer's disease. Arch. Neurol. 50, 949–954.
Kim, K.S., Han, P.L., 2006. Optimization of chronic stress paradigms using anxiety- and depression-like behavioral parameters. J. Neurosci. Res. 83, 497–507.
Kuhn, H.G., Cooper-Kuhn, C.M., Boekhoorn, K., Lucassen, P.J., 2007. Changes in neurogenesis in dementia and Alzheimer mouse models: are they functionally relevant? Eur. Arch. Psychiatry Clin. Neurosci. 257, 281–289.
Maekawa, M., Takashima, N., Arai, Y., Nomura, T., Inokuchi, K., Yuasa, S., Osumi, N., 2005. Pax6 is required for production and maintenance of progenitor cells in postnatal hippocampal neurogenesis. Genes Cells 10, 1001–1014.
Masters, C.L., Beyreuther, K., 1998. Alzheimer's disease. British Med. J. 316, 446–448.
Mattson, M.P., 2004. Pathways towards and away from Alzheimer's disease. Nature 430, 631–639.
Nacher, J., Varea, E., Blasco-Ibañez, J.M., Castillo-Gomez, E., Crespo, C., Martinez-Guijarro, F.J., McEwen, B.S., 2005. Expression of the transcription factor Pax 6 in the adult rat dentate gyrus. J. Neurosci. Res. 81, 753–761.
Nagata, K., Nakashima-Kamimura, N., Mikami, T., Ohsawa, I., Ohta, S., 2009. Consumption of molecular hydrogen prevents the stress-induced impairments in hippocampus-dependent learning tasks during chronic physical restraint in mice. Neuropsychopharmacology 34, 501–508.
Naruse, S., Thinakaran, G., Luo, J.J., Kusiak, J.W., Tomita, T., Iwatsubo, T., Qian, X., Ginty, D.D., Price, D.L., Borchelt, D.R., Wong, P.C., Sisodia, S.S., 1998. Effects of PS1 deficiency on membrane protein trafficking in neurons. Neuron 21, 1213–1221.
Ogita, K., Nishiyama, N., Sugiyama, C., Higuchi, K., Yoneyama, M., Yoneda, Y., 2005. Regeneration of granule neurons after lesioning of hippocampal dentate gyrus: evaluation using adult mice treated with trimethyltin chloride as a model. J. Neurosci. Res. 82, 609–621.
Osumi, N., Shinohara, H., Numayama-Tsuruta, K., Maekawa, M., 2008. Concise review: Pax6 transcription factor contributes to both embryonic and adult neurogenesis as a multifunctional regulator. Stem Cells 26, 1663–1672.
Pardon, M.C., Rattray, I., 2008. What do we know about the long-term consequences of stress on ageing and the progression of age-related neurodegenerative disorders? Neurosci. Biobehav. Rev. 32, 1103–1120.
Paxinos, G., Franklin, K.B., 2001. The Mouse Brain in Stereotaxic Coordinates, 2nd edn. Academic Press, San Diego.
Rao, M.S., Shetty, A.K., 2004. Efficacy of doublecortin as a marker to analyse the absolute number and dendritic growth of newly generated neurons in the adult dentate gyrus. Eur. J. Neurosci. 19, 234–246.
Rosenbrock, H., Koros, E., Bloching, A., Podhorna, J., Borsini, F., 2005. Effect of chronic intermittent restraint stress on hippocampal expression of marker proteins for synaptic plasticity and progenitor cell proliferation in rats. Brain Res. 1040, 55–63.
Sandi, C., 2004. Stress, cognitive impairment and cell adhesion molecules. Nat. Rev. Neurosci. 5, 917–930.
Shors, T.J., Miesegaes, G., Beylin, A., Zhao, M., Rydel, T., Gould, E., 2001. Neurogenesis in the adult is involved in the formation of trace memories. Nature 410, 372–376.
Veena, J., Srikumar, B.N., Mahati, K., Bhagya, V., Raju, T.R., Shankaranarayana Rao, B.S., 2009. Enriched environment restores hippocampal cell proliferation and ameliorates cognitive deficits in chronically stressed rats. J. Neurosci. Res. 87, 831–843.
von Bohlen Und Halbach, O., 2007. Immunohistological markers for staging neurogenesis in adult hippocampus. Cell Tissue Res. 329, 409–420.
Wen, P.H., Friedrich Jr., V.L., Shioi, J., Robakis, N.K., Elder, G.A., 2002. Presenilin-1 is expressed in neural progenitor cells in the hippocampus of adult mice. Neurosci. Lett. 318, 53–56.
Winner, B., Desplats, P., Hagl, C., Klucken, J., Aigner, R., Ploetz, S., Laemke, J., Karl, A., Aigner, L., Masliah, E., Buerger, E., Winkler, J., 2009. Dopamine receptor activation promotes adult neurogenesis in an acute Parkinson model. Exp. Neurol. 219, 543–552.
Zhang, C.L., Zou, Y., He, W., Gage, F.H., Evans, R.M., 2008. A role for adult TLX-positive neural stem cells in learning and behaviour. Nature 451, 1004–1007.
Zhang, C., McNeil, E., Dressler, L., Siman, R., 2007. Long-lasting impairment in hippocampal neurogenesis associated with amyloid deposition in a knock-in mouse model of familial Alzheimer's disease. Exp. Neurol. 204, 77–87.

Neurochemistry International 54 (2009) 330–338

Contents lists available at ScienceDirect

Neurochemistry International

journal homepage: www.elsevier.com/locate/neuint

Proteomic and histochemical analysis of proteins involved in the dying-back-type of axonal degeneration in the gracile axonal dystrophy (*gad*) mouse

Akiko Goto [a,b], Yu-Lai Wang [a], Tomohiro Kabuta [a], Rieko Setsuie [a], Hitoshi Osaka [a], Akira Sawa [c], Shoichi Ishiura [b], Keiji Wada [a,*]

[a] Department of Degenerative Neurological Diseases, National Institute of Neuroscience, National Center of Neurology and Psychiatry, 4-1-1 Ogawahigashi, Kodaira, Tokyo, 187-8502, Japan
[b] Department of Life Sciences, Graduate School of Arts and Sciences, University of Tokyo, 3-8-1 Komaba, Meguro-ku, Tokyo,153-8902, Japan
[c] Depts. of Psychiatry and Neuroscience, Johns Hopkins University School of Medicine, Baltimore, MD 21287, USA

ARTICLE INFO

Article history:
Received 24 November 2008
Received in revised form 12 December 2008
Accepted 17 December 2008
Available online 25 December 2008

Keywords:
Axonal degeneration
Dying-back
gad mouse
UCH-L1
Ubiquitin
2D-DIGE
GAPDH
Oxidative stress

ABSTRACT

Local axonal degeneration is a common pathological feature of peripheral neuropathies and neurodegenerative disorders of the central nervous system, including Alzheimer's disease, Parkinson's disease, and stroke; however, the underlying molecular mechanism is not known. Here, we analyzed the gracile axonal dystrophy (*gad*) mouse, which displays the dying-back-type of axonal degeneration in sensory neurons, to find the molecules involved in the mechanism of axonal degeneration. The *gad* mouse is analogous to a null mutant of ubiquitin carboxyl-terminal hydrolase L1 (UCH-L1). UCH-L1 is a deubiquitinating enzyme expressed at high levels in neurons, as well as testis and ovary. In addition, we recently discovered a new function of UCH-L1—namely to bind to and stabilize mono-ubiquitin in neurons, and found that the level of mono-ubiquitin was decreased in neurons, especially in axons of the sciatic nerve, in *gad* mice. The low level of ubiquitin suggests that the target proteins of the ubiquitin proteasome system are not sufficiently ubiquitinated and thus degraded in the *gad* mouse; therefore, these proteins may be the key molecules involved in axonal degeneration. To identify molecules involved in axonal degeneration in *gad* mice, we compared protein expression in sciatic nerves between *gad* and wild-type mice at 2 and 12 weeks old, using two-dimensional difference gel electrophoresis. As a result, we found age-dependent accumulation of several proteins, including glyceraldehyde-3-phosphate dehydrogenase (GAPDH) and 14-3-3, in *gad* mice compared with wild-type mice. Histochemical analyses demonstrated that GAPDH and 14-3-3 were localized throughout axons in both *gad* and wild-type mice, but GAPDH accumulated in the axons of *gad* mice. Recently, it has been suggested that a wide range of neurodegenerative diseases are characterized by the accumulation of intracellular and extracellular protein aggregates, and it has been reported that oxidative stress causes the aggregation of GAPDH. Furthermore, histochemical analysis demonstrated that sulfonated GAPDH, a sensor of oxidative stress that elicits cellular dysfunction, was expressed in the axons of *gad* mice, and 4-hydroxy-2-nonenal, a major marker of oxidative stress, was also only detected in *gad* mice. Our findings suggest that GAPDH may participate in a process of the dying-back-type of axonal degeneration in *gad* mice and may provide valuable insight into the mechanisms of axonal degeneration.

1. Introduction

Axonal degeneration occurs in several chronic neurodegenerative diseases and in injuries caused by, for example, toxic, ischemic, or traumatic insults. Recent findings suggest that axonal degeneration precedes, and sometimes causes, neuronal death in these neurodegenerative disorders (Li et al., 2001; Ferri et al., 2003; Fischer et al., 2004; Stokin et al., 2005; Fischer and Glass, 2007), but the underlying molecular mechanism is not known.

The gracile axonal dystrophy (*gad*) mutant mouse is characterized by sensory ataxia at an early stage, followed by motor ataxia at a later stage (Yamazaki et al., 1988; Saigoh et al., 1999). Pathologically, axonal degeneration in the *gad* mouse begins with the distal ends of primary ascending axons in the dorsal root ganglia (DRG) (Mukoyama et al., 1989; Kikuchi et al., 1990; Oda et al., 1992; Miura et al., 1993), and spheroid formation in the dying-back-type of axonal degeneration is observed in the gracile and dorsal spinocerebellar tracts (Yamazaki et al., 1988; Kikuchi

* Corresponding author. Tel.: +81 42 346 1715 fax: +81 42 346 1745.
E-mail address: wada@ncnp.go.jp (K. Wada).

0197-0186/$ – see front matter © 2008 Elsevier Ltd. All rights reserved.
doi:10.1016/j.neuint.2008.12.012

et al., 1990; Miura et al., 1993). At a later stage, axonal degeneration and spheroid formation are observed at both the central and peripheral ends of DRG neurons and extend transsynaptically to the upper tracts as well as to motor neurons (Mukoyama et al., 1989; Kikuchi et al., 1990; Oda et al., 1992; Miura et al., 1993). Therefore, the *gad* mouse is an effective model for analyzing the molecular mechanism of the dying-back-type of axonal degeneration.

Previously, we found that the *gad* mutation is caused by an in-frame deletion of *Uchl1*, which encodes ubiquitin carboxyl-terminal hydrolase L1 (UCH-L1) (Saigoh et al., 1999). UCH-L1 is expressed at high levels in neurons, as well as testis and ovary, and constitutes ~5% of total soluble protein in the brain (Wilkinson et al., 1989). UCH-L1 is reported to be one of the deubiquitinating enzymes in the ubiquitin-proteasome system (UPS), where it hydrolyzes bonds between ubiquitin (Ub) and small adducts and creates free mono-Ub *in vitro* (Larsen et al., 1998). UCH-L1 also acts as a Ub ligase *in vitro* (Liu et al., 2002). In addition, we recently found a new function for UCH-L1—to bind to and stabilize mono-Ub in neurons (Osaka et al., 2003).

Using histochemical analysis, we previously demonstrated that UCH-L1 and mono-Ub are colocalized in axons of the sciatic nerve. In *gad* mice, the level of mono-Ub was decreased in neurons, especially in axons of the sciatic nerve (Osaka et al., 2003). The low level of ubiquitin suggests that the target proteins of the ubiquitin-proteasome system (UPS) are not sufficiently ubiquitinated and thus degraded in the *gad* mouse; therefore, these proteins may be key molecules involved in axonal degeneration. To identify the molecules involved in axonal degeneration in *gad* mice, we analyzed protein expression in sciatic nerves using two-dimensional difference gel electrophoresis (2D-DIGE).

Proteomic approaches compare protein expression comprehensively; 2D-DIGE is a modification of the traditional 2D technology, in which small amounts of multiple protein samples can be compared together, because each sample can be pre-labeled with different fluorescence dyes, mixed together, and run on the same isoelectric focusing (IEF) gel and SDS-PAGE (Knowles et al., 2003; Shaw and Riederer, 2003). We used 2D-DIGE because it is the most efficient method for analyzing the small amount of protein that can be extracted from a sciatic nerve. Here, we show that there are age-dependent accumulations of several proteins, including glyceraldehyde-3-phosphate dehydrogenase (GAPDH) and 14-3-3, in *gad* mice compared with wild-type (WT) mice, suggesting that these proteins are involved in axonal degeneration.

2. Experimental procedures

2.1. Animals

We used homozygous *gad* mice and their wild-type siblings (Harada et al., 2004; Wang et al., 2004). Mice were maintained and propagated at the National Institute of Neuroscience, National Center of Neurology and Psychiatry, Japan. Proteomic studies were carried out at 2 and 12 weeks old. Western blotting analyses were carried out at 12 weeks old. Histochemical analyses were carried out at 7 and 12 weeks old. Animals were anesthetized with Nembutal, and the sciatic nerve was perfused with saline. All mouse experiments were performed in accordance with our institution's regulations for animal care and with the approval of the Animal Investigation Committee of the National Institute of Neuroscience, National Center of Neurology and Psychiatry which conforms to the National Institute of Health guide for the care and use of laboratory animals.

2.2. Preparation of protein samples and labeling of protein samples with Cy dyes

Each sciatic nerve was suspended in 300 μl of sample buffer, containing 7 M urea, 2 M thiourea, 4% (w/v) CHAPS, and 40 mM Tris base (pH 8.0), by sonication for 60 s on ice, gently vortexed, and centrifuged for 20 min at 14,000 × *g* at 4 °C. Protein concentration was determined using a 2-D Quant Kit (GE Healthcare, Piscataway, NJ, USA). Protein samples were labeled as recommended by the manufacturer (GE Healthcare) using 400 pmol Cy dyes (GE Healthcare) per 50 μg of protein. Separate solutions containing 15 μg of protein from one *gad* or WT sample were labeled with Cy3 or Cy5 dye, respectively, and a common pool of proteins with *gad* and WT samples mixed equally were labeled with Cy2 dye by vortexing and incubating on ice in the dark for 30 min. The labeled samples were quenched by the addition of 1 μl 10 mM lysine (Sigma–Aldrich, St. Louis, MO, USA) and incubated on ice for 10 min.

2.3. Two-dimensional polyacrylamide gel electrophoresis (2D PAGE)

The quenched Cy3, Cy5, and Cy2 samples (15 μg of protein each) were mixed and denatured in 2D PAGE sample buffer containing 7 M urea, 2 M thiourea, 4% (w/v) CHAPS, 0.2% DTT, and 1.4% Ampholine. For the IEF, 45 μg of protein was applied to a rehydrated Immobiline Drystrip (pH 3–10, 7 cm; GE Healthcare) in a strip holder and incubated overnight in the dark. IEF was performed using a Multiphor II Electrophoresis system (GE Healthcare). The electrophoresis conditions were set as follows: step 1, 200 V for 1 min; step 2, 3500 V for 90 min; step 3, 3500 V for 125 min. After IEF, the strip was equilibrated with SDS buffer and applied to the 12.5% 2D SDS-PAGE for the analysis of 12-week-old mice and to the 4–20% SDS-PAGE for the analysis of 2-week-old mice using a precast Multigel II system (Daiichi Kagaku, Japan).

2.4. Image analysis and statistics

We scanned 2D gels using a Typhoon 9000 fluorescent imager (GE Healthcare). Excitation/emission wavelengths were chosen for each of the dyes. Gel images were preprocessed to remove extraneous areas using ImageQuant V5.0 (GE Healthcare). Gel analysis was performed using DeCyder DIA V5.0 (Difference In-gel Analysis; GE Healthcare). In-gel matching and statistical analysis were performed using DeCyder BVA V5.0 (Biological Variance Analysis; GE Healthcare). The Student's paired *t*-test ($P < 0.05$) was performed to identify the protein spots that were differentially expressed between *gad* and WT mice.

2.5. In-gel digestion and analysis by matrix-assisted laser desorption/ionization tandem time-of-flight (MALDI-TOF/TOF) mass spectrometry

To identify a particular protein in a spot detected by 2D-DIGE analysis, sciatic nerve extract containing 100 μg of protein was subjected to 12.5% 2D SDS-PAGE and stained with Coomassie brilliant blue (Invitrogen). The spots of interest were excised from the gel, destained, dehydrated with acetonitrile for 10 min, and completely dried under a vacuum pump for 10 min. Each spot was placed in 20 μl of 5 mM NH_4HCO_3 containing 1 pmol of sequencing-grade trypsin (Promega, Madison, WI, USA) overnight at 37 °C. Aliquots of the trypsinized samples were analyzed by nanoliquid chromatography and automatically spotted with alpha-cyano-4-hydroxy-cinnamic acid solution on a stainless-steel target and air dried. All mass spectra were obtained with MALDI-TOF/TOF (AXIMA-CFR; Shimadzu, Japan). MALDI peptide spectra were calibrated using several peaks of self-digested trypsin and matrix ion as internal standards.

2.6. Protein identification

Protein identification was performed using database searches on the web with Mascot Wizard (Matrix Science Ltd., London, United Kingdom). Criteria for protein identification were as follows: mascot score higher than 80 and mass tolerance of 100 ppm. Calculated pI and molecular mass data were obtained by Mascot.

2.7. 2D Western blotting for identification of GAPDH

One protein spot that was increased in *gad* mice but could not be detected by MALDI-TOF/TOF analysis was speculated to be GAPDH from its isoelectric point, molecular weight and location of the 2D gel compared with the mouse brain proteome database, and was therefore subjected to 2D Western blotting using an anti-GAPDH antibody (1:200, Chemicon, MAB374). One-hundred μg of sciatic nerve proteins were separated by 12.5% 2D SDS-PAGE and transferred onto a PVDF membrane (Immobilon-P; Millipore, Bedford, MA, USA). The membrane was washed with MilliQ water for 1 h at room temperature. Western blotting was performed as described in the following section.

2.8. Western blotting

Using 4–20% gradient SDS-PAGE, 2 μg of total protein was separated and transferred onto a PVDF membrane (Immobilon-P; Millipore). The membrane was washed with MilliQ water, then blocked with 5% skim milk in 0.05% Tween 20 in TBS (TTBS) for 1 h at room temperature, and incubated with primary antibodies in TTBS overnight at 4 °C. Primary antibodies used in this study were anti-UCH-L1 polyclonal antibody (1:5000, UltraClone, RA95101), anti-GAPDH monoclonal antibody (1:200, Chemicon, MAB374), anti-14-3-3 polyclonal antibody (1:100, IBL, 18649), anti-neurofilament L monoclonal antibody (NF-L, 1:500, Chemicon, MAB1615), anti-neuronal class III β tubulin antibody (βTUBIII, 1:1000, Covance, TUJ1), and anti-actin monoclonal antibody (1:4000, Sigma, AC-15). After washing, the membranes were incubated for 1 h at room temperature with either anti-mouse or anti-rabbit IgG horseradish peroxidase (HRP) conjugated secondary antibodies (1:10,000, GE Healthcare). Protein signals were detected with SuperSignal West Femto Maximum Sensitivity Substrate (Pierce) and were visualized with the LAS-3000 imaging system (Fujifilm, Tokyo, Japan).

2.9. Immunohistochemistry

Mice were anesthetized and perfused with ice-cold 4% paraformaldehyde in phosphate-buffered saline (PBS, pH 7.4). Sciatic nerves were collected and postfixed in 4% paraformaldehyde overnight at 4 °C. The samples were embedded in paraffin and sectioned at 5 μm for immunohistochemistry. Serial sections were deparaffinized in xylene and graded ethanol, and washed in distilled water. Sections were blocked by incubation in 10% normal goat serum for 30 min at room temperature and incubated overnight at 4 °C with diluted primary antibodies. The following antibodies were used at the final dilutions indicated: anti-GAPDH polyclonal antibody (1:1000), anti-sulfonated GAPDH polyclonal antibody (1:500; these two antibodies were kindly provided by Dr. Sawa), anti-14-3-3 polyclonal antibody (1:100, IBL, 18649), anti-myelin basic protein monoclonal antibody (MBP, 1:200, QED Bioscience, 24201), anti-neurofilament M monoclonal antibody (NF-M, 1:200, Chemicon, MAB1621), anti-UCH-L1 polyclonal antibody (1:2000, UltraClone, RA95101), anti-UCH-L1 monoclonal antibody (1:200; Medac, Wedel, Germany), βTUBIII (1:300, COVANCE, TUJ1), and anti-4-hydroxy-2-nonenal monoclonal antibody (HNE, 25 μg/ml, JaICA, Shizuoka, Japan).

After incubating with primary antibodies, sections were washed 5 times with 0.1% Tween 20 in PBS (PBST) for 5 min at room temperature and then incubated for 90 min at room temperature with diluted secondary antibodies. The following antibodies were used at the final dilutions indicated: anti-mouse-Alexa594 IgG and anti-rabbit-Alexa588 IgG (1:400, Invitrogen) for immunofluorescence staining, or EnVision+ anti-rabbit HRP (Dako, Japan) for DAB staining. For DAB staining, bound antibody complexes were visualized using DAB (Dako, Japan) as a peroxidase substrate. Primary and secondary antibodies were diluted in Dako Antibody Diluent (Dako, Japan). After incubation with secondary antibodies, sections were washed 5 times with PBST for 5 min at room temperature and mounted with Antifade Kit (Molecular Probes). For analysis of 14-3-3 and HNE, sections were pretreated in a microwave oven for 10 min in citrate buffer solution (pH 6.0), cooled down, and washed 3 times for 5 min in PBS at room temperature. For the other immunostaining analyses, this pretreatment was not needed. For DAB staining, sections were treated with 3% H_2O_2 in methanol for 5 min to quench endogenous peroxidase activity before treatment with the primary antibodies.

3. Results

3.1. Analyses of differentially expressed proteins between gad and WT mice by 2D-DIGE

To find proteins that are upregulated in *gad* mice compared with WT mice, we analyzed sciatic nerves from 3 *gad* and 3 WT mice at 2 weeks old as well as at 12 weeks old, using 2D-DIGE technology. The proteins from *gad* mice were pre-labeled with Cy5 (red), and the proteins from WT mice were pre-labeled with Cy3 (green), respectively. A common pool of proteins composed of an equal amount of protein from a single *gad* and WT mouse was pre-labeled with Cy2, and the same manipulation was performed in 3 independent experiments.

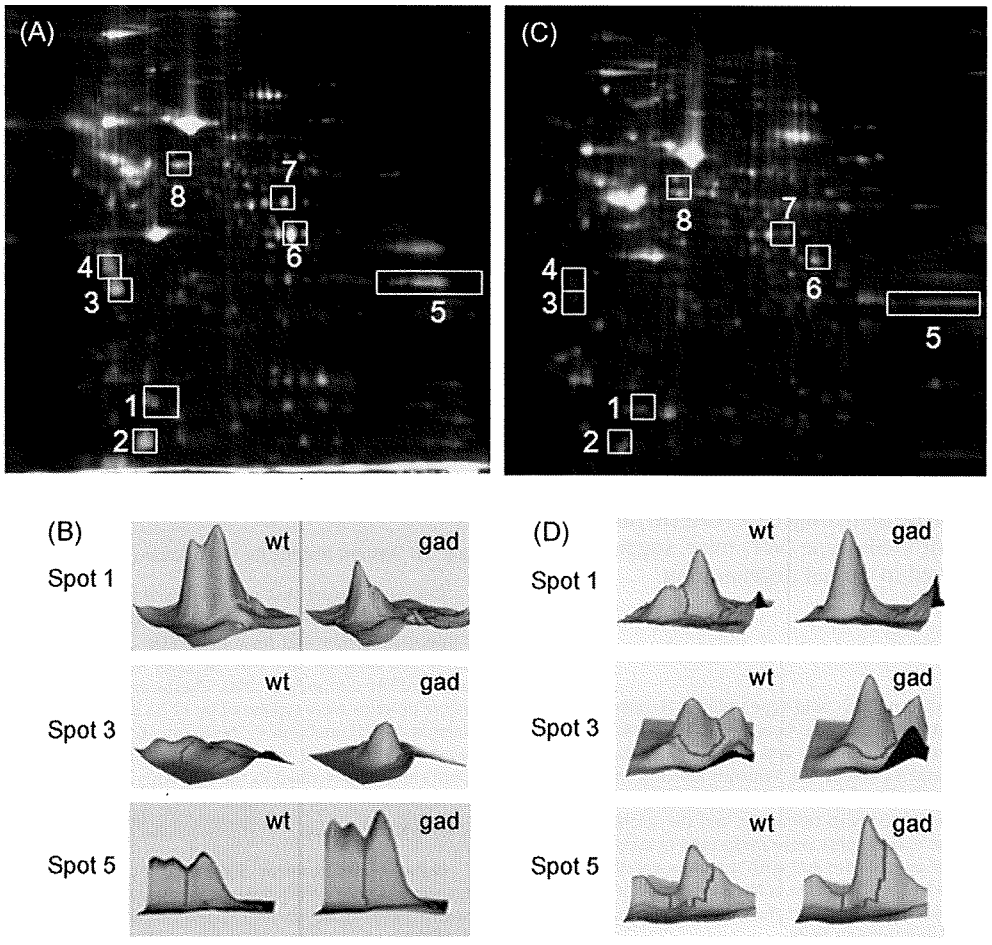

Fig. 1. Analyses of differentially expressed proteins between *gad* and wild-type mice by two-dimensional difference gel electrophoresis (2D-DIGE).
(A) A representative pseudocolor picture of superimposed DIGE images of mice at 12 weeks old. Fourteen protein spots are increased in *gad* mice compared with wild-type (WT) mice (red) by at least 1.6-fold (Student's paired *t*-test value; $P < 0.05$ in 3 parallel gels), and one spot is not detected at all in *gad* mice (green). Seven protein spots (spot No. 2–8) are increased in *gad* mice in an age-dependent manner, and one spot (spot No. 1) was not detected at all in *gad* mice at either 2 or 12 weeks old. The spot numbers of the latter differentiated 8 spots are shown in this map.
(B) A representative pseudocolor picture of superimposed DIGE images of mice at 2 weeks old. Eighteen protein spots are increased in *gad* mice compared with WT mice (red) by at least 1.6-fold (Student's paired *t*-test value; $P < 0.05$ in 3 parallel gels), and one spot is not detected at all in *gad* mice (green). The spot numbers in this figure are the same as in A.
(C) The 3D images of typical protein spots that were differentially expressed between *gad* and WT mice at 2 weeks old (spot numbers 1, 3, and 5 in A).
(D) The 3D images of typical protein spots that were differentially expressed between *gad* and WT mice at 2 weeks old (spot numbers 1, 3, and 5 in C) (For interpretation of the references to color in this figure legend, the reader is referred to the web version of the article.)

Table 1
List of proteins differentially expressed between *gad* and WT mice.

Spot no.	Protein name	Score	Molecular mass (kDa)/pI	Av. ratio (*gad*/wt) 12 weeks	*P* value	Av. ratio (*gad*/wt) 2 weeks	*P* value
1	Ubiquitin thiolesterase PGP9.5 (UCH-L1)	96	25.10/5.12	−14.38	0.005	−3.89	0.003
3	14-3-3 protein	94	28.10/4.63	5.4	0.030	7.32	0.001
4	Annexin A5	143	35.79/4.83	6.68	0.020	5.19	0.030
8	Neurofilament triplet L protein (NF-L)	212	61.40/4.62	2.18	0.010	3.53	0.026
5	Glyceraldehyde 3-phosphate dehydrogenase (GAPDH)		38.07/8.34	3.89	0.043	1.61	

*GAPDH was detected by 2D Western blotting and not by MALDI-TOF/TOF.

Fig. 1A shows a representative pseudocolor picture of superimposed DIGE images of the 12-week-old mouse samples. Fourteen protein spots were increased by at least 1.6-fold in *gad* mice compared with WT mice (red; Student's paired *t*-test value; $P < 0.05$ in 3 parallel gels), and one spot was not detected at all in *gad* mice (green).

Fig. 1B shows a representative pseudocolor picture of superimposed DIGE images of the 2-week-old mouse samples. Eighteen protein spots were increased by at least 1.6-fold in *gad* mice compared with WT mice (red; Student's paired *t*-test value; $P < 0.05$ in 3 parallel gels), and one spot was not detected at all in *gad* mice (green).

Based on comparison of the 2D-DIGE analysis of mice between 2 and 12 weeks old, 7 protein spots showed an age-dependent increase in *gad* mice (spots No. 2–8). One spot (spot No. 1) was not detected at all in *gad* mice at either 2 or 12 weeks old (Fig. 1A and B).

Fig. 1C shows the 3D images of typical spots (spots No. 1, 3, and 5) in Fig. 1A, and Fig. 1D shows the 3D images of typical spots (spots No. 1, 3, and 5) in Fig. 1B.

3.2. Identification of differentially expressed proteins between gad and WT mice by MALDI-TOF/TOF and 2D Western blotting

The proteins of spots that were age dependently increased or absent in *gad* mice were analyzed by MALDI-TOF/TOF and identified (spots No. 1, 3, 4, and 8). The proteins were identified as UCH-L1 (spot No. 1), 14-3-3 (spot No. 3), annexin V (spot No. 4), and Neurofilament L (NF-L) (spot No. 8). Additionally, we speculated that spot No. 5 may represent GAPDH based on the information from the mouse brain proteome database (http://www.charite.de/humangenetik/klose_public1/index.html), and confirmed this by 2D Western blotting with GAPDH antibodies. The results of the protein identification are listed in Table 1, including spot number, protein name, mascot score, theoretical relative molecular mass, isoelectric point, average ratio of *gad*/wt protein level, and *P*-value using DeCyder, at both 2 and 12 weeks old.

3.3. Analyses of the expression levels of proteins in gad and WT mice by Western blotting

In 2D-DIGE system, each sample was pre-labeled with different fluorescence dyes, Cy3, Cy5 or Cy2. This labeling-process allows comparison of multiple samples in same 2D-gel, but it is reported that efficiency of each dyes to label proteins was not exactly the same. We assume that 2D-DIGE is reliable method to detect molecules involved in axonal degeneration but Western blot analysis using specific antibodies is more accurate, and in fact, it is usual that identified proteins by TOF-MASS are reconfirmed by Western blotting. Therefore, the expression levels of the proteins in

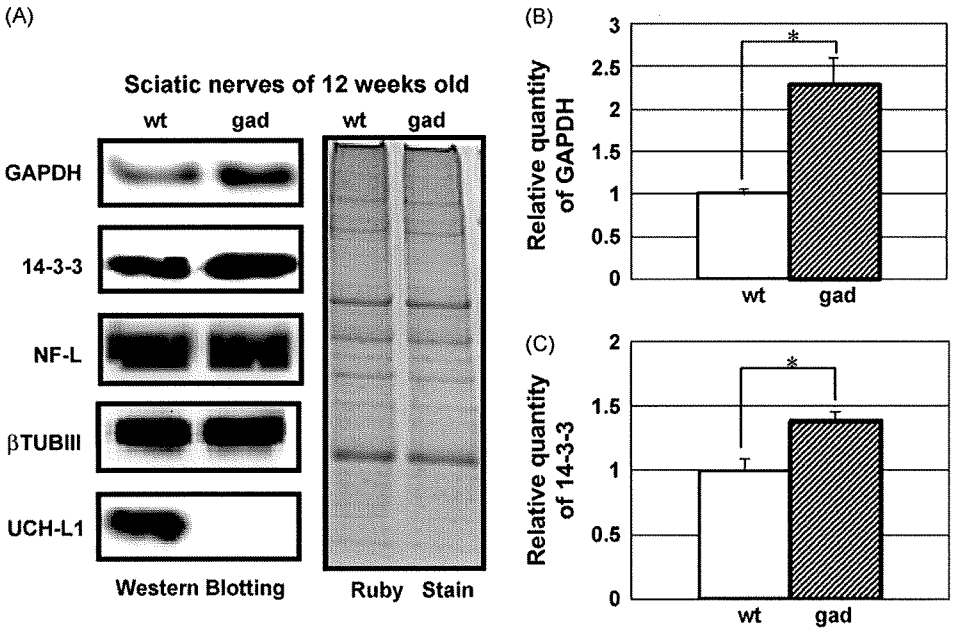

Fig. 2. Western blotting analyses of the expression levels of proteins expressed differentially between *gad* and WT mice.
(A) Results of Western blotting analysis with antibodies against ubiquitin carboxyl-terminal hydrolase L1 (UCH-L1), neurofilament L (NF-L), 14-3-3, glyceraldehyde-3-phosphate dehydrogenase (GAPDH), and classIII β tubulin (βTUBIII). GAPDH and 14-3-3 protein levels were increased in *gad* mice compared with WT mice.
(B) Quantification of the band intensities of GAPDH. Values are means ± SEM of 3 independent experiments (*$P < 0.05$); GAPDH is increased by about 2.3-fold in *gad* mice at 12 weeks old compared with WT mice.
(C) Quantification of the band intensities of 14-3-3. Values are means ± SEM of 3 independent experiments (*$P < 0.05$); 14-3-3 is increased by 1.3-fold in *gad* mice at 12 weeks old compared with WT mice.

gad and WT mice listed in Table 1 were further analyzed by Western blotting to reconfirm the results of 2D-DIGE (Fig. 2A). We chose these proteins because they were all reported to be expressed in neurons. In 12-week-old *gad* mice, GAPDH was increased by an average ratio of 2.3-fold (Fig. 2B), and 14-3-3 was increased by an average ratio of 1.3-fold (Fig. 2C) compared with WT mice. The levels of NF-L and βTUBIII, which was used as an internal control, showed no significant difference between *gad* and WT mice at 12 weeks old (Fig. 2A). Annexin V was not analyzed because its antibodies did not work in this experimental system containing urea and thiourea. The same results were obtained in 3 independent experiments.

3.4. Histochemical localization of GAPDH in the sciatic nerves of gad and WT mice

Sciatic nerves are composed internally of neuronal axons and externally of myelin derived from glial Schwann cells, and protein samples in the proteomic analysis were a mixture of axons and myelin. We examined the histological localization of GAPDH, which was dominantly increased in *gad* mice, by double immunofluorescence staining using an antibody against GAPDH and the neuronal markers neurofilament M (NF-M) or UCH-L1, or the Schwann cells marker myelin basic protein (MBP). In *gad* mice, GAPDH was colocalized with MBP (Fig. 3A, right panel) but was more dominantly colocalized with NF-M, a neuronal marker (Fig. 3A, left panel). These results suggest that GAPDH is mainly localized in axons in *gad* mice. In WT mice, GAPDH was colocalized with the neuronal marker UCH-L1 (Fig. 3B, left panel). Because UCH-L1 is the product of the gene defective in the *gad* mouse, UCH-L1 is not detected in *gad* mice (Fig. 3B, right panel). The same results were obtained in 3 independent experiments.

3.5. DAB staining analyses of GAPDH and 14-3-3 in the sciatic nerves of gad and WT mice

We examined in detail the localization of GAPDH in cross or vertical sections of sciatic nerve axons by DAB staining (Figs. 4A–F). In the cross-sections, GAPDH was localized in axons in both *gad* and WT mice and was remarkably accumulated in *gad* mice compared with WT mice (Fig. 4A and B). In vertical sections, GAPDH was also localized in axons in both *gad* and WT mice (Fig. 4C–F). Notably, aggregates of GAPDH were observed in *gad* mice but not in WT mice (Fig. 4E and F, arrow). Next, we examined the expression of 14-3-3, which was found to be increased in *gad* mice upon 2D-DIGE and Western blotting analyses. In both *gad* and WT mice, 14-3-3 was expressed in axons, and there was no significant difference between *gad* and WT mice (Fig. 4G–J). The same results were obtained in 3 independent experiments.

3.6. Histochemical analyses of sulfonated GAPDH in the sciatic nerves of gad and WT mice

It was reported that oxidative stress induces the oligomerization and aggregation of GAPDH (Cumming and Schubert, 2005; Nakajima et al., 2007), and in this study we found that GAPDH is accumulated in axons of *gad* mice that exhibit a dying-back-type of axonal degeneration. Thus, we postulated that oxidative stress would be increased in *gad* mice, and therefore examined the expression of sulfonated GAPDH (Hara et al., 2005), in the sciatic

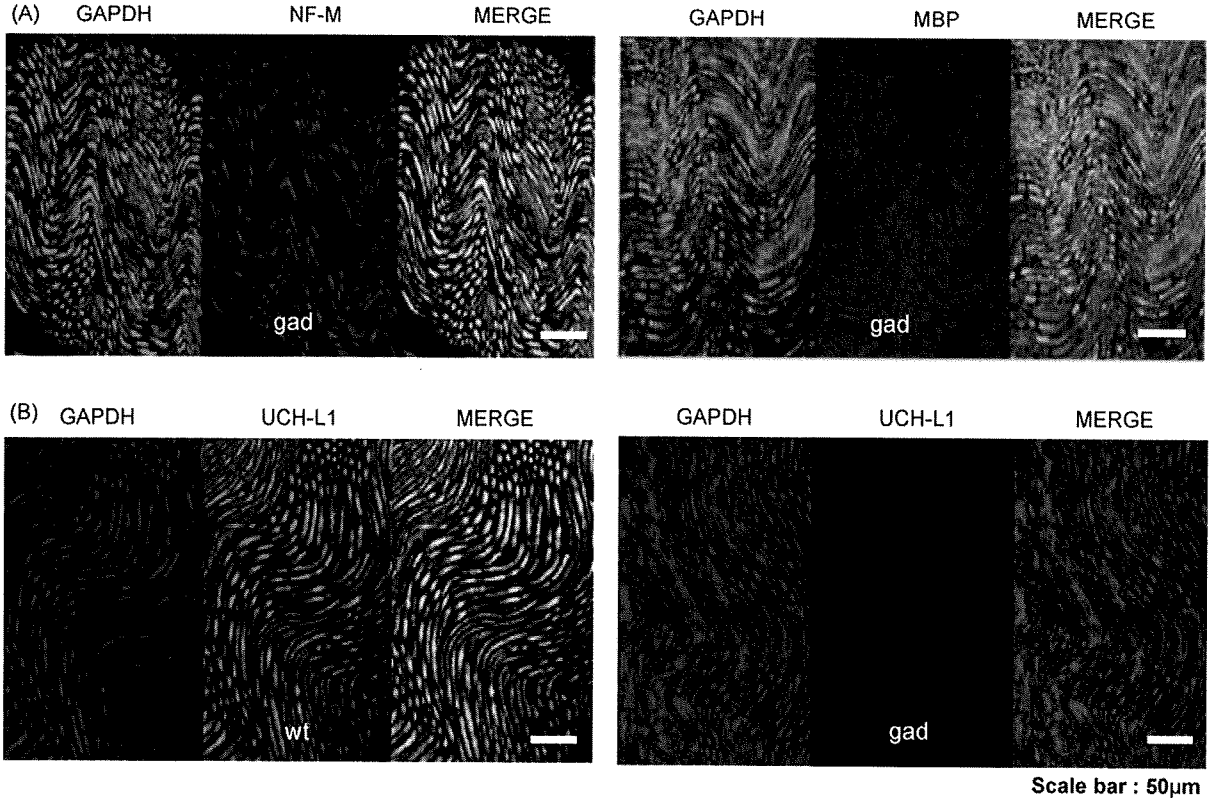

Fig. 3. Histochemical localization of GAPDH in the sciatic nerves of *gad* and WT mice.
(A) Double immunofluorescent staining of the sciatic nerve of *gad* mice using antibodies against GAPDH, neurofilament M (NF-M), or myelin basic protein (MBP). GAPDH was colocalized with NF-M (left panel) and partly with MBP (right panel) in *gad* mice. GAPDH is mainly localized in axons.
(B) Double immunofluorescent staining of the sciatic nerve of *gad* and WT mice using antibodies against GAPDH and UCH-L1. In WT mice, GAPDH is colocalized with UCH-L1 (left panel). In *gad* mice, UCH-L1 is not detected (right panel), and GAPDH is strongly detected compared with WT mice.

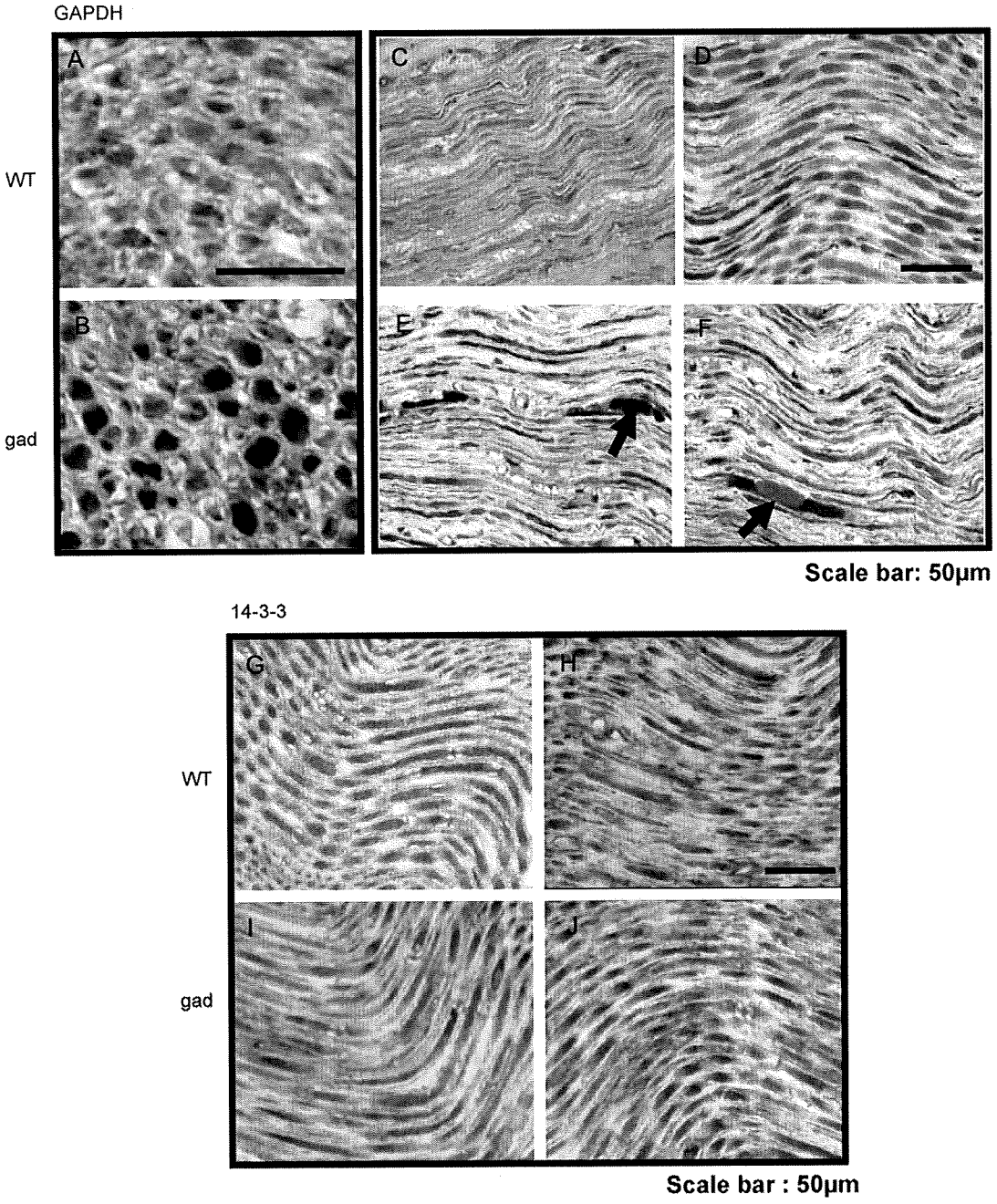

Fig. 4. DAB staining of GAPDH and 14-3-3 in the sciatic nerves of *gad* and WT mice.
(A–F) Sections of sciatic nerves of WT (A, C, and D) or *gad* (B, E, and F) mice stained with DAB using GAPDH antibodies.
(A) Cross-section of a sciatic nerve of a WT mouse. GAPDH is mainly localized in axons.
(B) Cross-section of a sciatic nerve of a *gad* mouse. GAPDH is mainly localized in axons and is highly expressed compared with the WT mouse.
(C and D) Vertical sections of sciatic nerves of WT mice. GAPDH is localized in axons.
(E and F) Vertical sections of sciatic nerves of *gad* mice. GAPDH is localized in axons and is accumulated. GAPDH aggregates are indicated by arrows.
(G–J) Sections of sciatic nerves of WT (G, H) and *gad* (I, J) mice stained with DAB using 14-3-3 antibodies.
(G and H) Vertical sections of sciatic nerves of WT mice; 14-3-3 is localized in axons of WT mice.
(I and J) Vertical sections of sciatic nerves of *gad* mice; 14-3-3 is localized in axons of *gad* mice, and there was no significant difference between *gad* and WT mice (G, H).

nerves of *gad* and WT mice. We found that although sulfonated GAPDH was not detected in WT mice, it was clearly detected in *gad* mice (Fig. 5A and B). In *gad* mice, sulfonated GAPDH was colocalized with the neuronal markers βTUBIII (Fig. 5B) and NF-M (data not shown) in axons. In *gad* mice, accumulated sulfonated GAPDH was also detected in the outer portion of the axons, around the DAPI staining for nuclei (Fig. 5C). Axons do not contain nuclei, so these DAPI signals may come from Schwann cells. The same results were obtained in 3 independent experiments.

3.7. Histological analyses of HNE, a marker of oxidative stress, in the sciatic nerves of gad and WT mice

The results shown in Fig. 5 suggest that the level of oxidative stress is increased in *gad* mice. Accordingly, we examined the existence of HNE, a major marker of oxidative stress, in addition to sulfonated GAPDH. HNE was detected in *gad* mice, but not in WT mice (Fig. 6). The same results were obtained in 3 independent experiments.

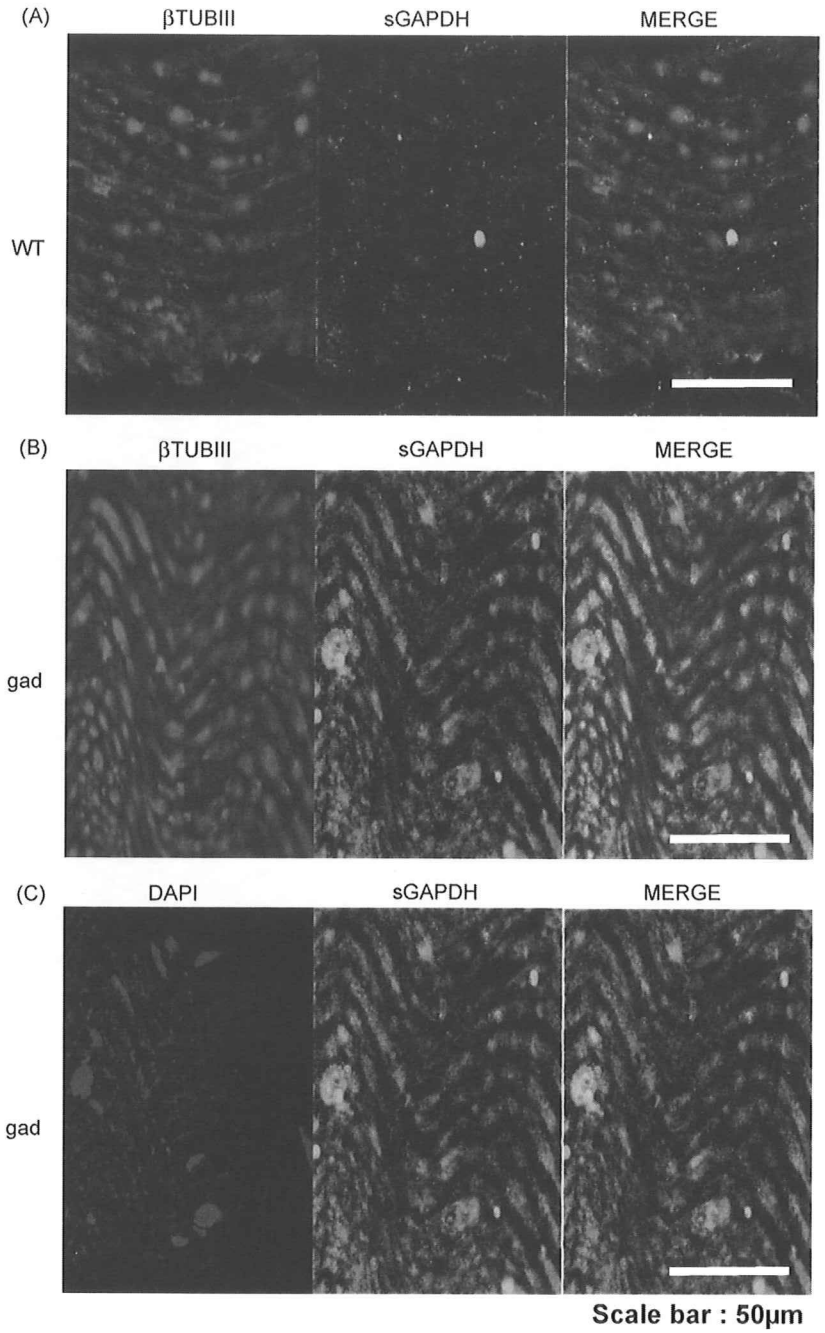

Fig. 5. Expression of sulfonated GAPDH in the sciatic nerves of *gad* and WT mice.
(A) Double immunofluorescent staining of a sciatic nerve of a WT mouse using antibodies against sulfonated GAPDH and βTUBIII. Sulfonated GAPDH was not detected in WT mice (middle panel).
(B) Double immunofluorescent staining of a sciatic nerve of a *gad* mouse using antibodies against sulfonated GAPDH and βTUBIII. In *gad* mice, sulfonated GAPDH was detected in axons of sciatic nerves (middle panel). Sulfonated GAPDH was colocalized with the neuronal marker βTUBIII in *gad* mice (right panel), as well as NF-M (data not shown). A representative result from 3 independent experiments is shown.
(C) Double immunofluorescent staining of a sciatic nerve of the *gad* mouse using an antibody against sulfonated GAPDH and DAPI. Sulfonated GAPDH was detected uniformaly within the axons of *gad* mice, and accumulation of sulfonated GAPDH was detected around the DAPI signals (right panel).

4. Discussion

In this study, we found that 14-3-3, annexin V, NF-L, and GAPDH were increased in an age-dependent manner in *gad* mice that display the dying-back-type of axonal degeneration, using 2D-DIGE analyses (Fig. 1). Based on Western blotting analyses, 14-3-3 and GAPDH were increased in *gad* mice compared with WT mice (Fig. 2). Histochemical analysis revealed that GAPDH was localized throughout axons and was accumulated in axons in *gad* mice compared with WT mice (Figs. 3 and 4). Also 14-3-3 was localized throughout axons, but there was no significant difference between *gad* and WT mice upon histochemical analyses, although it was increased in *gad* mice upon Western blotting analyses (Fig. 4). Since Western blotting showed only a slight increase in 14-3-3 (Fig. 2), we assume that this small difference could not be detected by histochemical analyses.

GAPDH is a classic glycolytic enzyme (Sirover, 1999; Chuang et al., 2005), and recent studies show that it is multifunctional

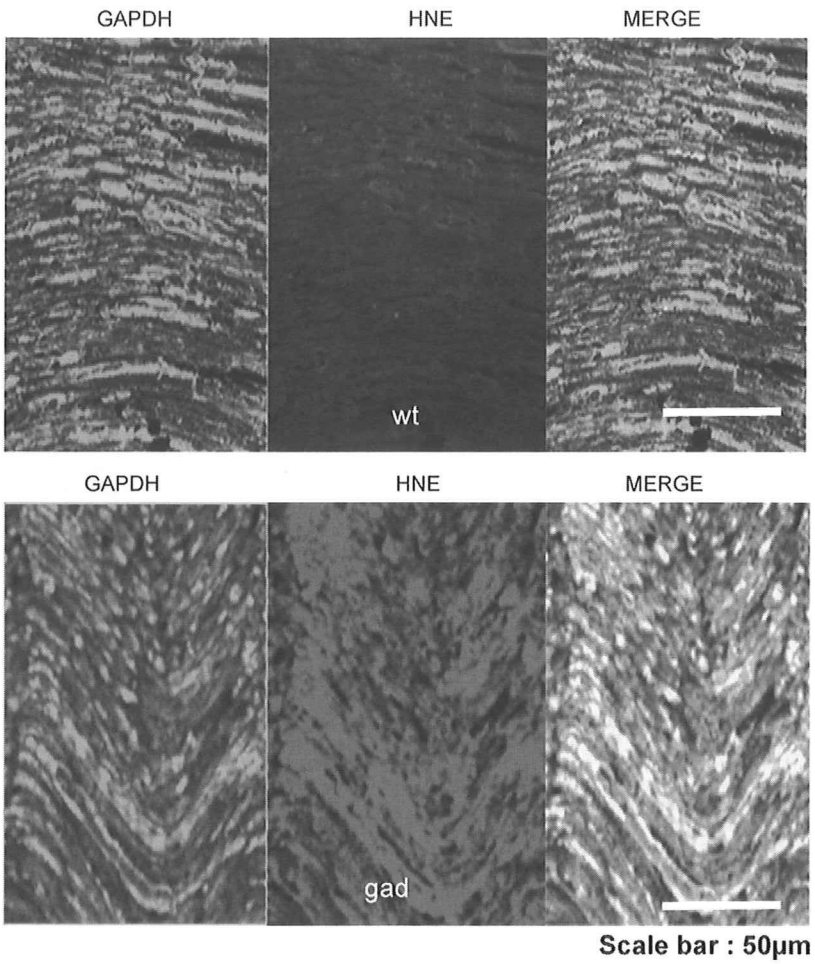

Fig. 6. Expression of HNE, a marker of oxidative stress, in the sciatic nerves of *gad* and WT mice.
Double immunofluorescent staining of sciatic nerves of *gad* and WT mice using antibodies against GAPDH and HNE. In WT mice, HNE was not detected (upper panel). On the other hand, HNE was strongly detected and mainly colocalized with GAPDH in *gad* mice (lower panel).

(Hara et al., 2006a). GAPDH has been reported to play roles in membrane fusion, microtubule bundling, nuclear RNA transport (Sirover, 1999), and transcription (Zheng et al., 2003). Particularly, its role as a mediator for cellular dysfunction/death has been highlighted (Sawa et al., 1997; Ishitani et al., 1998; Hara et al., 2005, 2006b). Sulfonation of GAPDH is reported to be induced by oxidative stress, and sulfonated GAPDH leads to cellular dysfunction (Hara et al., 2005, 2006a; Sen et al., 2008). Additionally, oxidative stress induces the oligomerization and aggregation of GAPDH through aberrant disulfide bonding of active-site cysteines, which leads to the formation of insoluble aggregates *in vitro* (Cumming and Schubert, 2005; Nakajima et al., 2007). Thus, GAPDH appears to participate in the mechanism leading to cellular dysfunction/death induced by oxidative stress. However, its function in axons or its association with axonal degeneration has not yet been demonstrated.

In this study, we found that GAPDH and sulfonated GAPDH were accumulated in *gad* mice compared with WT mice, suggesting that oxidative stress is increased in *gad* mice. In fact, we found that the oxidative stress marker HNE is increased in *gad* mice. It has also been reported that, the levels of carbonyl modification of proteins that is caused by oxidative stress are increased in the brains of *gad* mice compared with WT mice (Castegna et al., 2004). Therefore, we assume that accumulation of GAPDH and sulfonated GAPDH in the axons of *gad* mice were induced by oxidative stress.

Various molecules are involved in reduction-oxidative reactions, and recently the necessity of the UPS in reduction-oxidative reactions has been highlighted (Okada et al., 1999; Kang et al., 2008). It has been reported that a number of oxidative stress sensors are regulated by the UPS (Iwai, 2003; Kobayashi et al., 2004; Hara et al., 2006a). In *gad* mice, free-Ub pools are decreased in neurons, and proteolysis in the UPS is thought to be abnormal (Osaka et al., 2003). Oxidative stress is therefore expected to be increased in *gad* mice, which is consistent with our findings.

There is another possible mechanism for the accumulation of GAPDH in the axons of *gad* mice. GAPDH is reported to be degraded mainly by chaperone-mediated autophagy (Aniento et al., 1993; Cuervo et al., 1997). Our recent study showed that UCH-L1 physically interacts with lysosome-associated membrane protein type 2A, which is a component of CMA (Kabuta et al., 2008); thus CMA is possibly altered in the neuronal system of *gad* mice, potentially leading to the accumulation of GAPDH in the axons of *gad* mice.

This study demonstrates the alteration of GAPDH in axons of the *gad* mouse, a mutant with a loss of function of UCH-L1. Our findings suggest that GAPDH may participate in the process leading to the dying-back-type of axonal degeneration in *gad* mice and may provide valuable insight into the mechanisms of axonal degeneration.

Acknowledgements

We thank the following people for their contributions to this work: Dr. Hidemitsu Nakajima (Osaka Prefecture University), Dr. Satoshi Nagamine (National Center of Neurology and Psychiatry) and Dr. Makoto R. Hara (Johns Hopkins University School of Medicine) for helpful discussions; Ms. Hisae Kikuchi (National Center of Neurology and Psychiatry) for technical assistance with tissue sections; Ms. Masako Shikama (National Center of Neurology and Psychiatry) for the care and breeding of animals; Dr. Hayato Onishi (University of Tokyo) for assistance with the TOF MASS analysis; and Dr. H. Akiko Popiel (National Center of Neurology and Psychiatry) for support with English; Mitsubishi Tanabe Pharma Corporation for giving a chance to A.G. of admission to doctoral course. This work was supported in part by Grants-in-Aid for Scientific Research from the Ministry of Health, Labour and Welfare of Japan, Grants-in-Aid for Scientific Research from the Ministry of Education, Culture, Sports, Science and Technology of Japan, the Program for Promotion of Fundamental Studies in Health Sciences of the National Institute of Biomedical Innovation, and a grant from Japan Science and Technology Agency.

References

Aniento, F., Roche, E., Cuervo, A.M., Knecht, E., 1993. Uptake and degradation of glyceraldehyde-3-phosphate dehydrogenase by rat liver lysosomes. J. Biol. Chem. 268, 10463–10470.

Castegna, A., Thongboonkerd, V., Klein, J., Lynn, B.C., Wang, Y.L., Osaka, H., Wada, K., Butterfield, D.A., 2004. Proteomic analysis of brain proteins in the gracile axonal dystrophy (gad) mouse, a syndrome that emanates from dysfunctional ubiquitin carboxyl-terminal hydrolase L-1, reveals oxidation of key proteins. J. Neurochem. 88, 1540–1546.

Chuang, D.M., Hough, C., Senatorov, V.V., 2005. Glyceraldehyde-3-phosphate dehydrogenase, apoptosis, and neurodegenerative diseases. Annu. Rev. Pharmacol. Toxicol. 45, 269–290.

Cuervo, A.M., Dice, J.F., Knecht, E., 1997. A population of rat liver lysosomes responsible for the selective uptake and degradation of cytosolic proteins. J. Biol. Chem. 272, 5606–5615.

Cumming, R.C., Schubert, D., 2005. Amyloid-beta induces disulfide bonding and aggregation of GAPDH in Alzheimer's disease. FASEB J. 19, 2060–2062.

Ferri, A., Sanes, J.R., Coleman, M.P., Cunningham, J.M., Kato, A.C., 2003. Inhibiting axon degeneration and synapse loss attenuates apoptosis and disease progression in a mouse model of motoneuron disease. Curr. Biol. 13, 669–673.

Fischer, L.R., Culver, D.G., Tennant, P., Davis, A.A., Wang, M., Castellano-Sanchez, A., Khan, J., Polak, M.A., Glass, J.D., 2004. Amyotrophic lateral sclerosis is a distal axonopathy: evidence in mice and man. Exp. Neurol. 185, 232–240.

Fischer, L.R., Glass, J.D., 2007. Axonal degeneration in motor neuron disease. Neurodegener. Dis. 4, 431–442.

Hara, M.R., Agrawal, N., Kim, S.F., Cascio, M.B., Fujimuro, M., Ozeki, Y., Takahashi, M., Cheah, J.H., Tankou, S.K., Hester, L.D., Ferris, C.D., Hayward, S.D., Snyder, S.H., Sawa, A., 2005. S-nitrosylated GAPDH initiates apoptotic cell death by nuclear translocation following Siah1 binding. Nat. Cell. Biol. 7, 665–674.

Hara, M.R., Cascio, M.B., Sawa, A., 2006a. GAPDH as a sensor of NO stress. Biochim. Biophys. Acta 1762, 502–509.

Hara, M.R., Thomas, B., Cascio, M.B., Bae, B.I., Hester, L.D., Dawson, V.L., Dawson, T.M., Sawa, A., Snyder, S.H., 2006b. Neuroprotection by pharmacologic blockade of the GAPDH death cascade. Proc. Natl. Acad. Sci. U.S.A. 103, 3887–3889.

Harada, T., Harada, C., Wang, Y.L., Osaka, H., Amanai, K., Tanaka, K., Takizawa, S., Setsuie, R., Sakurai, M., Sato, Y., Noda, M., Wada, K., 2004. Role of ubiquitin carboxy terminal hydrolase-L1 in neural cell apoptosis induced by ischemic retinal injury in vivo. Am. J. Pathol. 164, 59–64.

Ishitani, R., Tanaka, M., Sunaga, K., Katsube, N., Chuang, D.M., 1998. Nuclear localization of overexpressed glyceraldehyde-3-phosphate dehydrogenase in cultured cerebellar neurons undergoing apoptosis. Mol. Pharmacol. 53, 701–707.

Iwai, K., 2003. An ubiquitin ligase recognizing a protein oxidized by iron: implications for the turnover of oxidatively damaged proteins. J. Biochem. 134, 175–182.

Kabuta, T., Furuta, A., Aoki, S., Furuta, K., Wada, K., 2008. Aberrant interaction between Parkinson disease-associated mutant UCH-L1 and the lysosomal receptor for chaperone-mediated autophagy. J. Biol. Chem. 283, 23731–23738.

Kang, S.I., Choi, H.W., Kim, I.Y., 2008. Redox-mediated modification of PLZF by SUMO-1 and ubiquitin. Biochem. Biophys. Res. Commun. 369, 1209–1214.

Kikuchi, T., Mukoyama, M., Yamazaki, K., Moriya, H., 1990. Axonal degeneration of ascending sensory neurons in gracile axonal dystrophy mutant mouse. Acta Neuropathol. 80, 145–151.

Knowles, M.R., Cervino, S., Skynner, H.A., Hunt, S.P., de Felipe, C., Salim, K., Meneses-Lorente, G., McAllister, G., Guest, P.C., 2003. Multiplex proteomic analysis by two-dimensional differential in-gel electrophoresis. Proteomics 3, 1162–1171.

Kobayashi, A., Kang, M.I., Okawa, H., Ohtsuji, M., Zenke, Y., Chiba, T., Igarashi, K., Yamamoto, M., 2004. Oxidative stress sensor Keap1 functions as an adaptor for Cul3-based E3 ligase to regulate proteasomal degradation of Nrf2. Mol. Cell. Biol. 24, 7130–7139.

Larsen, C.N., Krantz, B.A., Wilkinson, K.D., 1998. Substrate specificity of deubiquitinating enzymes: ubiquitin C-terminal hydrolases. Biochemistry 37, 3358–3368.

Li, H., Li, S.H., Yu, Z.X., Shelbourne, P., Li, X.J., 2001. Huntingtin aggregate-associated axonal degeneration is an early pathological event in Huntington's disease mice. J. Neurosci. 21, 8473–8481.

Liu, Y., Fallon, L., Lashuel, H.A., Liu, Z., Lansbury Jr., P.T., 2002. The UCH-L1 gene encodes two opposing enzymatic activities that affect alpha-synuclein degradation and Parkinson's disease susceptibility. Cell 111, 209–218.

Miura, H., Oda, K., Endo, C., Yamazaki, K., Shibasaki, H., Kikuchi, T., 1993. Progressive degeneration of motor nerve terminals in GAD mutant mouse with hereditary sensory axonopathy. Neuropathol. Appl. Neurobiol. 19, 41–51.

Mukoyama, M., Yamazaki, K., Kikuchi, T., Tomita, T., 1989. Neuropathology of gracile axonal dystrophy (GAD) mouse. An animal model of central distal axonopathy in primary sensory neurons. Acta Neuropathol. 79, 294–299.

Nakajima, H., Amano, W., Fujita, A., Fukuhara, A., Azuma, Y.T., Hata, F., Inui, T., Takeuchi, T., 2007. The active site cysteine of the proapoptotic protein glyceraldehyde-3-phosphate dehydrogenase is essential in oxidative stress-induced aggregation and cell death. J. Biol. Chem. 282, 26562–26574.

Oda, K., Yamazaki, K., Miura, H., Shibasaki, H., Kikuchi, T., 1992. Dying back type axonal degeneration of sensory nerve terminals in muscle spindles of the gracile axonal dystrophy (GAD) mutant mouse. Neuropathol. Appl. Neurobiol. 18, 265–281.

Okada, K., Wangpoengtrakul, C., Osawa, T., Toyokuni, S., Tanaka, K., Uchida, K., 1999. 4-Hydroxy-2-nonenal-mediated impairment of intracellular proteolysis during oxidative stress. Identification of proteasomes as target molecules. J. Biol. Chem. 274, 23787–23793.

Osaka, H., Wang, Y.L., Takada, K., Takizawa, S., Setsuie, R., Li, H., Sato, Y., Nishikawa, K., Sun, Y.J., Sakurai, M., Harada, T., Hara, Y., Kimura, I., Chiba, S., Namikawa, K., Kiyama, H., Noda, M., Aoki, S., Wada, K., 2003. Ubiquitin carboxy-terminal hydrolase L1 binds to and stabilizes monoubiquitin in neuron. Hum. Mol. Genet. 12, 1945–1958.

Saigoh, K., Wang, Y.L., Suh, J.G., Yamanishi, T., Sakai, Y., Kiyosawa, H., Harada, T., Ichihara, N., Wakana, S., Kikuchi, T., Wada, K., 1999. Intragenic deletion in the gene encoding ubiquitin carboxy-terminal hydrolase in gad mice. Nat. Genet. 23, 47–51.

Sawa, A., Khan, A.A., Hester, L.D., Snyder, S.H., 1997. Glyceraldehyde-3-phosphate dehydrogenase: nuclear translocation participates in neuronal and nonneuronal cell death. Proc. Natl. Acad. Sci. U.S.A. 94, 11669–11674.

Sen, N., Hara, M.R., Kornberg, M.D., Cascio, M.B., Bae, B.I., Shahani, N., Thomas, B., Dawson, T.M., Dawson, V.L., Snyder, S.H., Sawa, A., 2008. Nitric oxide-induced nuclear GAPDH activates p300/CBP and mediates apoptosis. Nat. Cell. Biol. 10, 866–873.

Shaw, M.M., Riederer, B.M., 2003. Sample preparation for two-dimensional gel electrophoresis. Proteomics 3, 1408–1417.

Sirover, M.A., 1999. New insights into an old protein: the functional diversity of mammalian glyceraldehyde-3-phosphate dehydrogenase. Biochim. Biophys. Acta 1432, 159–184.

Stokin, G.B., Lillo, C., Falzone, T.L., Brusch, R.G., Rockenstein, E., Mount, S.L., Raman, R., Davies, P., Masliah, E., Williams, D.S., Goldstein, L.S., 2005. Axonopathy and transport deficits early in the pathogenesis of Alzheimer's disease. Science 307, 1282–1288.

Wang, Y.L., Takeda, A., Osaka, H., Hara, Y., Furuta, A., Setsuie, R., Sun, Y.J., Kwon, J., Sato, Y., Sakurai, M., Noda, M., Yoshikawa, Y., Wada, K., 2004. Accumulation of beta- and gamma-synucleins in the ubiquitin carboxyl-terminal hydrolase L1-deficient gad mouse. Brain Res. 1019, 1–9.

Wilkinson, K.D., Lee, K.M., Deshpande, S., Duerksen-Hughes, P., Boss, J.M., Pohl, J., 1989. The neuron-specific protein PGP 9.5 is a ubiquitin carboxyl-terminal hydrolase. Science 246, 670–673.

Yamazaki, K., Wakasugi, N., Tomita, T., Kikuchi, T., Mukoyama, M., Ando, K., 1988. Gracile axonal dystrophy (GAD), a new neurological mutant in the mouse. Proc. Soc. Exp. Biol. Med. 187, 209–215.

Zheng, L., Roeder, R.G., Luo, Y., 2003. S phase activation of the histone H2B promoter by OCA-S, a coactivator complex that contains GAPDH as a key component. Cell 114, 255–266.

J Neuropathol Exp Neurol

Vol. 68, No. 9
September 2009
pp. 994–1005

ORIGINAL ARTICLE

Abnormal Localization of Leucine-Rich Repeat Kinase 2 to the Endosomal-Lysosomal Compartment in Lewy Body Disease

Shinji Higashi, MD, PhD, Darren J. Moore, PhD, Ryoko Yamamoto, MD, PhD, Michiko Minegishi, PhD, Kiyoshi Sato, MD, PhD, Takashi Togo, MD, PhD, Omi Katsuse, MD, PhD, Hirotake Uchikado, MD, PhD, Yoshiko Furukawa, MD, PhD, Hiroaki Hino, MD, PhD, Kenji Kosaka, MD, PhD, Piers C. Emson, PhD, Keiji Wada, MD, PhD, Valina L. Dawson, PhD, Ted M. Dawson, MD, PhD, Heii Arai, MD, PhD, and Eizo Iseki, MD, PhD

Abstract

Missense mutations in the *leucine-rich repeat kinase 2* (*LRRK2*) gene are the most common causes of both familial and sporadic forms of Parkinson disease and are also associated with diverse pathological alterations. The mechanisms whereby *LRRK2* mutations cause these pathological phenotypes are unknown. We used immunohistochemistry with 3 distinct anti-LRRK2 antibodies to characterize the expression of LRRK2 in the brains of 21 subjects with various neurodegenerative disorders and 7 controls. The immunoreactivity of LRRK2 was localized in a subset of brainstem-type Lewy bodies (LBs) but not in cortical-type LBs, tau-positive inclusions, or TAR-DNA–binding protein-43–positive inclusions. The immunoreactivity of LRRK2 frequently appeared as enlarged granules or vacuoles within neurons of affected brain regions, including the substantia nigra, amygdala, and entorhinal cortex in patients with Parkinson disease or dementia with LBs. The volumes of LRRK2-positive granular structures in neurons of the entorhinal cortex were significantly increased in dementia with LBs brains compared with age-matched control brains ($p < 0.05$). Double immunolabeling demonstrated that these LRRK2-positive granular structures frequently colocalized with the late-endosomal marker Rab7B and occasionally with the lysosomal marker, the lysosomal-associated membrane protein 2. These results suggest that LRRK2 normally localizes to the endosomal-lysosomal compartment within morphologically altered neurons in neurodegenerative diseases, particularly in the brains of patients with LB diseases.

Key Words: Alzheimer disease, Dementia with Lewy bodies, Endosome, Leucine-rich repeat kinase 2, Lysosome, PARK8, Parkinson disease.

INTRODUCTION

Parkinson disease (PD), the second most common age-related neurodegenerative disorder after Alzheimer disease (AD), is characterized by neuronal degeneration with Lewy bodies (LBs) in the substantia nigra pars compacta that leads to dysfunction of the nigrostriatal dopaminergic pathway, striatal dopamine deficiency, and clinical parkinsonism. Although the etiology of PD is not known, genetic analysis has provided important new insights into its pathogenesis. Mutations in 6 genes are unambiguously associated with rare Mendelian forms of PD, including *α-synuclein* (1), *parkin* (2), *PTEN-induced putative kinase 1 (PINK1)* (3), *DJ-1* (4), *leucine-rich repeat kinase 2 (LRRK2)* (5, 6), and *ATP13A2* (7). Of these genes, missense mutations in *LRRK2* have been identified as the cause of late-onset autosomal-dominant parkinsonism linked to chromosome 12q11.2-q13.1 (PARK8 locus). A G2019S mutation in *LRRK2*, which is the most prevalent *LRRK2* variant, also accounts for apparently sporadic cases with PD (8). The disease penetrance in PD subjects with *LRRK2* mutations seems to be age dependent (9), and their clinical and neurochemical manifestations are not different from those of idiopathic PD subjects. More important, in some ethnic subgroups including North African Arabs, Ashkenazi Jews, and Arab-Berbers of Tunisia, there is a higher frequency of the G2019S variant in PD cohorts (10, 11). Therefore, the LRRK2 protein may provide important insights into the pathogenesis of PD. At present, however, the biologic and functional roles of the LRRK2 protein are not well characterized.

From the PET/CT Dementia Research Center, Juntendo Tokyo Koto Geriatric Medical Center, Juntendo University School of Medicine, Koto-ku (SH, RY, MM, KS, EI); Department of Degenerative Neurological Diseases, National Institute of Neuroscience, National Center of Neurology and Psychiatry, Kodaira-shi (SH, KW), Tokyo; Yokohama Houyuu Hospital, Asahi-ku, Yokohama (SH, HH, KK), Japan; Laboratory of Molecular Neurodegenerative Research, Brain Mind Institute, Ecole Polytechnique Fédérale de Lausanne, Lausanne, Switzerland (DJM); Department of Psychiatry, Juntendo University School of Medicine, Bunkyo-ku, Tokyo (RY, HA); Department of Psychiatry, Yokohama City University School of Medicine, Kanazawa-ku, Yokohama (TT, OK, HU, YF), Japan; Laboratory of Molecular Neuroscience, The Babraham Institute, Babraham, Cambridge, UK (PCE); Neuroregeneration and Stem Cell Programs, Institute for Cell Engineering (VLD, TMD), Departments of Neurology (VLD, TMD), Neuroscience (VLD, TMD), and Physiology (VLD), Johns Hopkins University School of Medicine, Baltimore, Maryland.

Send correspondence and reprint requests to: Shinji Higashi, MD, PhD, Department of Degenerative Neurological Diseases, National Institute of Neuroscience, National Center of Neurology and Psychiatry, 4-1-1 Ogawa-Higashi, Kodaira-shi, Tokyo 187-8502, Japan; E-mail: higashis@ncnp.go.jp

This research was supported by grants from the Kurata Memorial Hitachi Science and Technology Foundation (Shinji Higashi); Grants-in-Aid for Young Scientists (B), Grant No. 21790856 (Shinji Higashi), from the Japan Ministry of Education, Science, Sports and Culture (Eizo Iseko); Grant No. NS38377 (Ted M. Dawson) from the National Institutes of Health/National Institute of Neurological Disorders and Stroke; and by funding support from the Ecole Polytechnique Fédérale de Lausanne (Darren J. Moore).